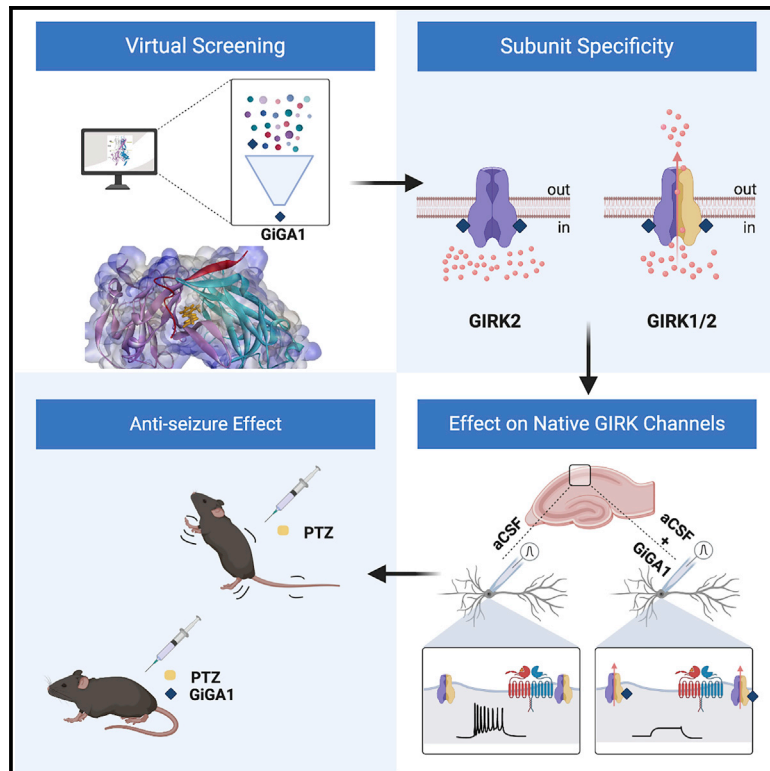


Identification of a G-Protein-Independent Activator of GIRK Channels

Graphical Abstract



Authors

Yulin Zhao, Peter Man-Un Ung, Gergely Zahoránszky-Kóhalmi, ..., Avner Schlessinger, Juan J. Marugan, Paul A. Slesinger

Correspondence

paul.slesinger@mssm.edu

In Brief

Zhao et al. identify GiGA1 through a virtual screen of ~750,000 chemical compounds using a high-resolution model of the alcohol pocket in GIRK channels. GiGA1 selectively activates GIRK1-containing channels and is G protein independent, like alcohol. GiGA1 activates endogenous GIRK channels in the brain and suppresses induced seizures.

Highlights

- Virtual screening with a GIRK alcohol pocket reveals a GIRK1-selective activator
- GiGA1 activates the GIRK channel directly without G proteins
- Natively expressed GIRK channels in the hippocampus are activated by GiGA1
- Systemic GiGA1 application reduces seizures in a convulsant animal model



Article

Identification of a G-Protein-Independent Activator of GIRK Channels

Yulin Zhao,¹ Peter Man-Un Ung,^{2,4} Gergely Zahoránszky-Kóhalmi,³ Alexey V. Zakharov,³ Natalia J. Martinez,³ Anton Simeonov,³ Ian W. Glaaser,¹ Ganesh Rai,³ Avner Schlessinger,² Juan J. Marugan,³ and Paul A. Slesinger^{1,5,*}¹Nash Family Department of Neuroscience, Icahn School of Medicine at Mount Sinai, New York, NY 10029, USA²Department of Pharmacological Sciences, Icahn School of Medicine at Mount Sinai, New York, NY 10029, USA³National Center for Advancing Translational Sciences (NCATS), Rockville, MD 20850, USA⁴Present address: Department of Discovery Chemistry, Genentech, Inc., South San Francisco, CA 94080, USA⁵Lead Contact

*Correspondence: paul.slesinger@mssm.edu

<https://doi.org/10.1016/j.celrep.2020.107770>

SUMMARY

G-protein-gated inwardly rectifying K⁺ (GIRK) channels are essential effectors of inhibitory neurotransmission in the brain. GIRK channels have been implicated in diseases with abnormal neuronal excitability, including epilepsy and addiction. GIRK channels are tetramers composed of either the same subunit (e.g., homotetramers) or different subunits (e.g., heterotetramers). Compounds that specifically target subsets of GIRK channels *in vivo* are lacking. Previous studies have shown that alcohol directly activates GIRK channels through a hydrophobic pocket located in the cytoplasmic domain of the channel. Here, we report the identification and functional characterization of a GIRK1-selective activator, termed GiGA1, that targets the alcohol pocket. GiGA1 activates GIRK1/GIRK2 both *in vitro* and *in vivo* and, in turn, mitigates the effects of a convulsant in an acute epilepsy mouse model. These results shed light on the structure-based development of subunit-specific GIRK modulators that could provide potential treatments for brain disorders.

INTRODUCTION

As members of the large inwardly rectifying potassium (K⁺) channel family, activation of G-protein-gated inwardly rectifying K⁺ (GIRK) channels hyperpolarizes cells by conducting a small outward K⁺ current near the resting membrane potential (RMP). This outward current underlies the metabotropic-dependent, slow inhibitory postsynaptic currents found in most brain regions (Lüscher and Slesinger, 2010; Luján and Aguado, 2015). Upon neurotransmitter-dependent activation of G-protein-coupled receptors (GPCRs), G_{α_{i/o}}-βγ heterotrimeric G proteins dissociate, allowing Gβγ subunits to directly activate GIRK channels (Aryal et al., 2009; Dascal, 1997; Reuveny et al., 1994; Yamada et al., 1998). Four mammalian GIRK channel subunits assemble as heterotetrameric channels (e.g., GIRK1/GIRK2, GIRK1/GIRK4, and GIRK2/GIRK3) and, in the case of GIRK2 and GIRK4, form homotetramers. GIRK1, GIRK2, and GIRK3 comprise the major GIRK subunits in the brain, whereas GIRK1/GIRK4 are expressed in the heart (Lesage et al., 1995; Wickman et al., 2000; Hibino et al., 2010; Lüscher and Slesinger, 2010). In the brain, different GIRK subunit combinations show distinct localization and expression patterns (Kobayashi et al., 1995; Karschin et al., 1996). GIRK1/GIRK2 heterotetramers are the predominant form of GIRK channels in the brain (Liao et al., 1996), except in the ventral tegmental area (VTA) dopamine neurons, which only express GIRK2 and GIRK3 subunits, and substantia nigra dopamine neurons, which only express GIRK2a/c subunits (Inanobe

et al., 1999; Cruz et al., 2004). Recent high-throughput screening (HTS) studies have identified some GIRK modulators (Kaufmann et al., 2013), but the limited number of GIRK subtype-specific compounds has hindered our understanding of the physiological role of GIRK channels in specific brain regions.

GIRK channels play an essential role in maintaining the RMP (Lüscher et al., 1997) and have been implicated in the pathophysiology of several diseases. For example, excessive GIRK channel activity can considerably reduce neuronal activity, such as described in Down syndrome, which contains a duplication of the chromosome containing KCNJ6 (GIRK2) (Reeves et al., 1995; Harashima et al., 2006; Best et al., 2007). The involvement of GIRK channels in neuronal death in Parkinson's disease was first characterized in the weaver GIRK2 mutant mouse (Liao et al., 1996; Surmeier et al., 1996; Slesinger et al., 1997). Moreover, several studies have identified mutations in GIRK2 that cause loss of ion selectivity. Aberrant Na⁺ flux through mutant GIRK channels trigger cell death, leading to physical abnormalities, developmental delay, and intellectual disabilities in severe hyperkinetic movement disorder patients, such as in Keppen-Lubinsky syndrome (Masotti et al., 2015; Horvath et al., 2018). In addition to gain-of-function-related diseases, knockout (KO) experiments in mice establish the importance of GIRK channels in preventing abnormal neuronal excitability. For instance, GIRK2 KO mice show susceptibility to γ-aminobutyric acid type A (GABA_A) receptor antagonist-induced seizures (Signorini et al., 1997). To date, none of the



commercially available anticonvulsive drugs specifically target the GIRK channel (Goldenberg, 2010).

In addition to G-protein-mediated activation, the GIRK channel can be directly activated by alcohols, such as ethanol and propanol (PrOH), through a G-protein-independent pathway (Kobayashi et al., 1999; Lewohl et al., 1999). An alcohol binding pocket was initially observed in an atomic structure of the Kir2.1 cytoplasmic domain (Pegan et al., 2006). Subsequently, the homologous pocket was identified in GIRK2 and characterized by mutagenesis and alcohol tagging studies, underscoring the significance of this pocket in the activation of GIRK channels (Aryal et al., 2009; Bodhinathan and Slesinger, 2013). These findings presented us with an opportunity to rationally design small molecules that target this alcohol binding pocket and modulate the activity of GIRK channels.

Here we describe the discovery and characterization of a GIRK1-specific channel modulator, which we refer to as G-protein-independent GIRK channel activator 1 (GiGA1). GiGA1 activates the GIRK1/GIRK2 channel in both heterologous expression systems and native neurons. Unlike previously characterized GIRK1 activators (Kaufmann et al., 2013), GiGA1 possesses alcohol-like kinetics of fast on and off rates. Moreover, our results suggest GiGA1 has a distinct mechanism of activation involving amino acids located within and near the alcohol pocket. By activating GIRK1/GIRK2 heterotetramers, GiGA1 can suppress the excitability of hippocampal CA1 pyramidal neurons. Moreover, in a pentylenetetrazol (PTZ)-induced model of epilepsy, we show *in vivo* efficacy for GiGA1 as an anticonvulsant.

RESULTS

Identification of GIRK Modulators from Homology Modeling and Structure-Based Virtual Screening against an Alcohol Pocket in GIRK2

To search for potential modulators of GIRK channels (Aryal et al., 2009; Bodhinathan and Slesinger, 2013), we first constructed a structural model of an alcohol pocket in GIRK2 for virtual screening. The alcohol pocket in GIRK channels is composed of three cytoplasmic domains (N terminus, β L- β M loop, β D- β E loop) at the interface of two adjoining subunits (Aryal et al., 2009). The alcohol pocket is partially visible in the full-length GIRK2 structures (PDB: 3SYA, 3SYQ, and 4KFM), but the region of the N terminus that forms one side of the alcohol binding pocket (residues 50–55) is disordered (PDB: 3SYA, 3SYQ, and 4KFM) (Figure 1Ai). To visualize a more complete GIRK2 alcohol pocket, we built a homology model of the GIRK2 cytoplasmic domain using MODELLER (Šali and Blundell, 1993) from the Kir2.1-methyl-pentane-diol (MPD) crystal structure (PDB: 2GIX) (Pegan et al., 2006) as a modeling template (Figure 1Aii). The cytoplasmic domain of Kir2.1 shares a sequence identity of 61% and a nearly identical structure with GIRK2 (root-mean-square deviation [RMSD] of 0.58 Å), with the residues corresponding to GIRK2 residues 50–55 resolved. To identify small molecules that are similar in size to MPD and would fit the allosteric site, we virtually screened the fragment-like subset of the ZINC15 (Sterling and Irwin, 2015) small-molecule library against the model of

the GIRK2 alcohol pocket, with constraints focusing on including a hydrophobic interaction constraint near leucines at position 257 (Leu257), an essential position for alcohol action (Aryal et al., 2009), as well as hydrogen-bond constraints to backbone of Lys52 and Pro256 (Figure 1B). Compounds with a favorable docking score were examined and prioritized for experimental testing to assess their functional effects on GIRK channels transiently expressed in HEK293T cells using whole-cell patch-clamp recordings.

Nine compounds were selected and purchased based on commercial availability from the ZINC15 library, and two were found to have moderate inhibitory effects on GIRK2 homotetrameric channels at high concentrations (500 μ M) (data not shown). We then expanded our search by virtually screening a subset of the National Center for Advancing Translational Sciences (NCATS) small-molecule library using the model of the GIRK2 alcohol binding pocket. Of the 1,000 top compounds, we selected and tested 13 compounds based on their docking pose, using selection criteria similar to that described earlier (Figure 1C). Nine of the 13 compounds activated GIRK2 channels (Figures 1D and 1E; Table S1). We also tested the effect on GIRK1/GIRK2 heterotetramers and discovered that 1-(2,3-dimethylphenyl)-3-(thiophen-2-yl)urea (i.e., compound 2) activated GIRK1/GIRK2 channels by \sim 200% (Figures 1D and 1E), making this a promising candidate for modulation of GIRK1/GIRK2 channel *in vivo*.

To develop an initial structure-activity relationship (SAR) model and improve the potency and specificity of compound 2, we tested 4 analogs, varying the position or number of methyl groups on the phenyl ring (Figure 2A). The analogs were identified by performing a similarity search with the NCATS in-house application and applying a similarity threshold of Tanimoto similarity \geq 0.85 (Tanimoto, 1969). One of the analogs, compound 2.3, which we refer to as GiGA1, exhibited high specificity for activating GIRK1/GIRK2 channels (Figures 2A and 2B). The reversal potential measured for GiGA1-induced GIRK1/GIRK2 currents was close to the Nernst potential for K^+ and comparable to basal and PrOH-induced currents (Figure 2B, arrow). Moreover, the inward rectification property of GIRK1/GIRK2 was maintained in the presence of GiGA1 (Figure 2B). To explore possible mechanisms for GiGA1's selectivity for activating GIRK1/GIRK2 channels, we performed an induced-fit docking (IFD) of GiGA1 and its analogs to the GIRK1/GIRK2 alcohol pocket (see STAR Methods). The predicted binding mode of GiGA1 placed the *o*-methylphenyl moiety of GiGA1 close to GIRK1_{L233} and GIRK1_{F46}, thereby forming a π - π interaction (Figure 2C). This tight fitting of GiGA1 in the GIRK1/GIRK2 alcohol pocket may explain the weaker binding of GiGA1 analogs, compounds 2, 2.1, 2.2, and 2.4, because they all have an extra methyl group that would potentially clash with GIRK1 F46 and L233, rendering them less optimal in binding and activating GIRK1/GIRK2 channels.

Although GiGA1 was selected based on the binding mechanism of alcohol, it has significantly higher potency compared with PrOH (>100 mM), with an EC_{50} (i.e., 50% activation concentration) of 31 μ M (Figure 2D). Unlike alcohol activation, which does not saturate (Bodhinathan and Slesinger, 2014), the GiGA1 activation of GIRK1/GIRK2 channels does saturate

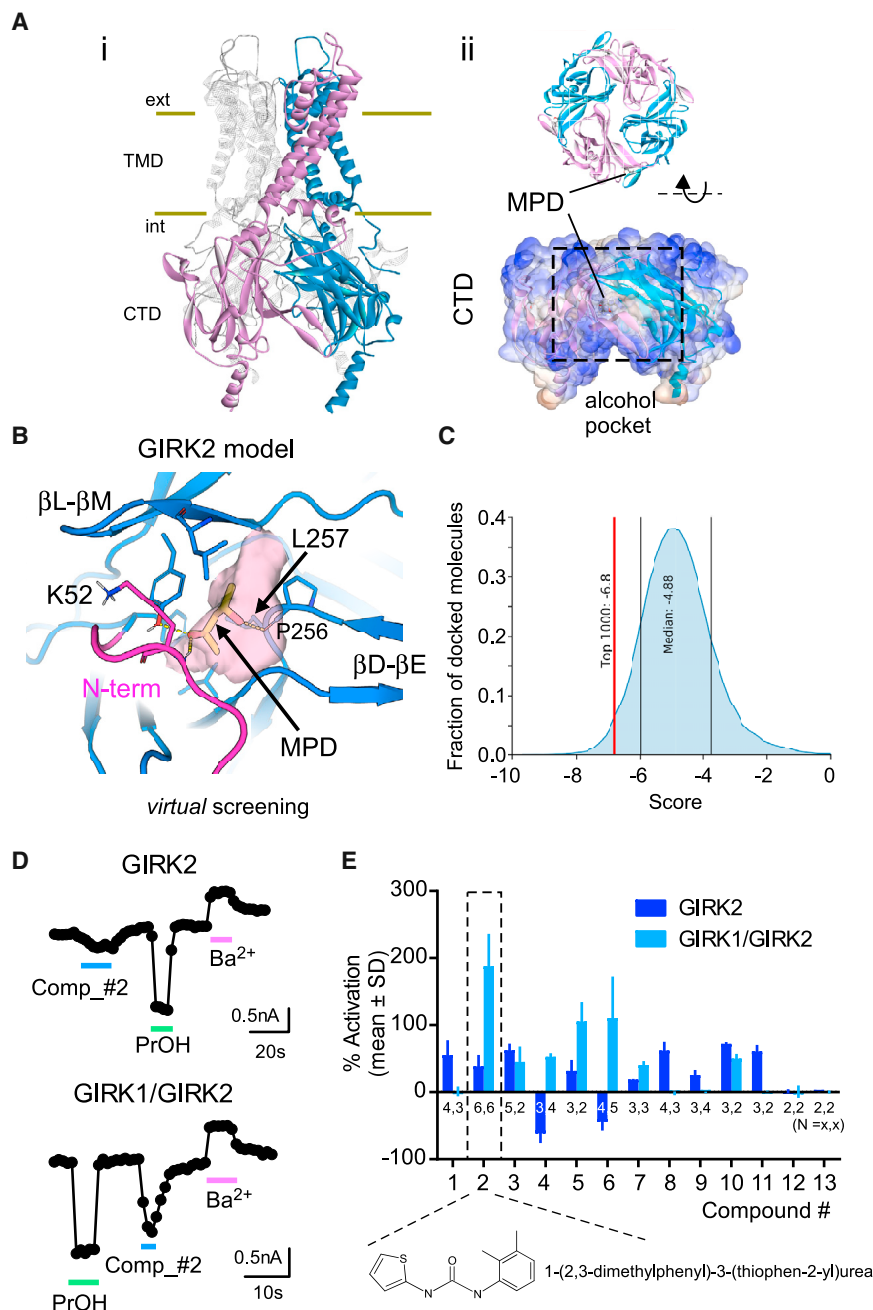


Figure 1. Discovery of GIRK Modulators through Structure-Based Virtual Screening of the GIRK2 Alcohol Pocket

(A) (i) Ribbon and surface views of homotetrameric GIRK2 (Whorton and MacKinnon, 2013). (ii) The alcohol pocket is located in the cytoplasmic domain (CTD) of the GIRK2 homology model. (B) Close view of the hydrophobic alcohol pocket (pink surface) between two subunits in the GIRK2 (blue cartoon) model (this study). The modeled N terminus is in magenta. MPD is indicated by yellow sticks. (C) Graph shows the normal distribution of docking scores of the screened NCATS compounds (56,834 molecules). The red line indicates the cutoff for the top 1,000 compounds. (D) Whole-cell patch-clamp recordings show the current response to PrOH (100 mM), compound 2 (100 μ M), and Ba^{2+} (1 mM) in cells transfected with GIRK2c cDNA (top) or GIRK1/GIRK2c tandem dimer cDNA (bottom). Currents were measured at -120 mV. (E) Bar graph shows the mean response, normalized to the Ba^{2+} -sensitive basal current (% activation), of compounds identified through virtual screening (see Table S1). Negative numbers indicate inhibition of GIRK channels. Compound 2 produced the largest activation of GIRK1/GIRK2 channels and was used for subsequent experiments (dashed box). n is indicated on the graph. Error bars represent SD on the graph.

at ~ 100 μ M (Figure 2D). Because GIRK subunits also assemble into other forms of GIRK channels in the brain and the heart, we next tested the effects of GiGA1 on GIRK2/GIRK3, GIRK1/GIRK3, and GIRK1/GIRK4 channels expressed in HEK293T cells. GiGA1 activated other GIRK1-containing GIRK channels, but not to the same extent as GIRK1/GIRK2 channels (Figure 2E). The specificity of PrOH was also tested on different GIRK channels and, consistent with previous studies (Kobayashi et al., 1999; Lewohl et al., 1999), PrOH was more potent in activating GIRK2-containing GIRK channels than other subtypes (Figure 2E).

fen-dependent activation was absent from cells expressing PTX S1, GiGA1 continued to activate GIRK1/GIRK2, similarly to PrOH, suggesting that G protein activation is not involved (Figures 3B and 3C).

To determine whether the site of action for GiGA1 involves the alcohol pocket of GIRK1/GIRK2, we examined the effects of a tryptophan substitution at Leu257, which was shown previously to directly attenuate alcohol activation (Figure S1) (Aryal et al., 2009). We sequentially mutated one or both Leu257 in GIRK2 and the homologous position 246 in GIRK1. Although neither activation of GiGA1 nor activation of PrOH was altered by a

Mechanism of GiGA1 Action on GIRK1-Containing GIRK Channels

GIRK channels are activated via a G-protein-dependent pathway in native cells (Dascal, 1997), and the alcohol pocket is located near the $G\beta\gamma$ binding domain of GIRK2 (PDB: 4KFM) (Bodhinathan and Slesinger, 2014) (Figure 3A). To investigate whether the effect of GiGA1 requires receptor-dependent G proteins, we co-expressed the pertussis toxin (PTX) S1 subunit with the γ -aminobutyric acid type B ($GABA_B$) heterodimer receptor and GIRK1/GIRK2 channels. The PTX S1 subunit ribosylates $G\alpha_{i/o}$ G proteins and uncouples them from receptors (Reisine, 1990) (Figure 3A). Whereas baclo-

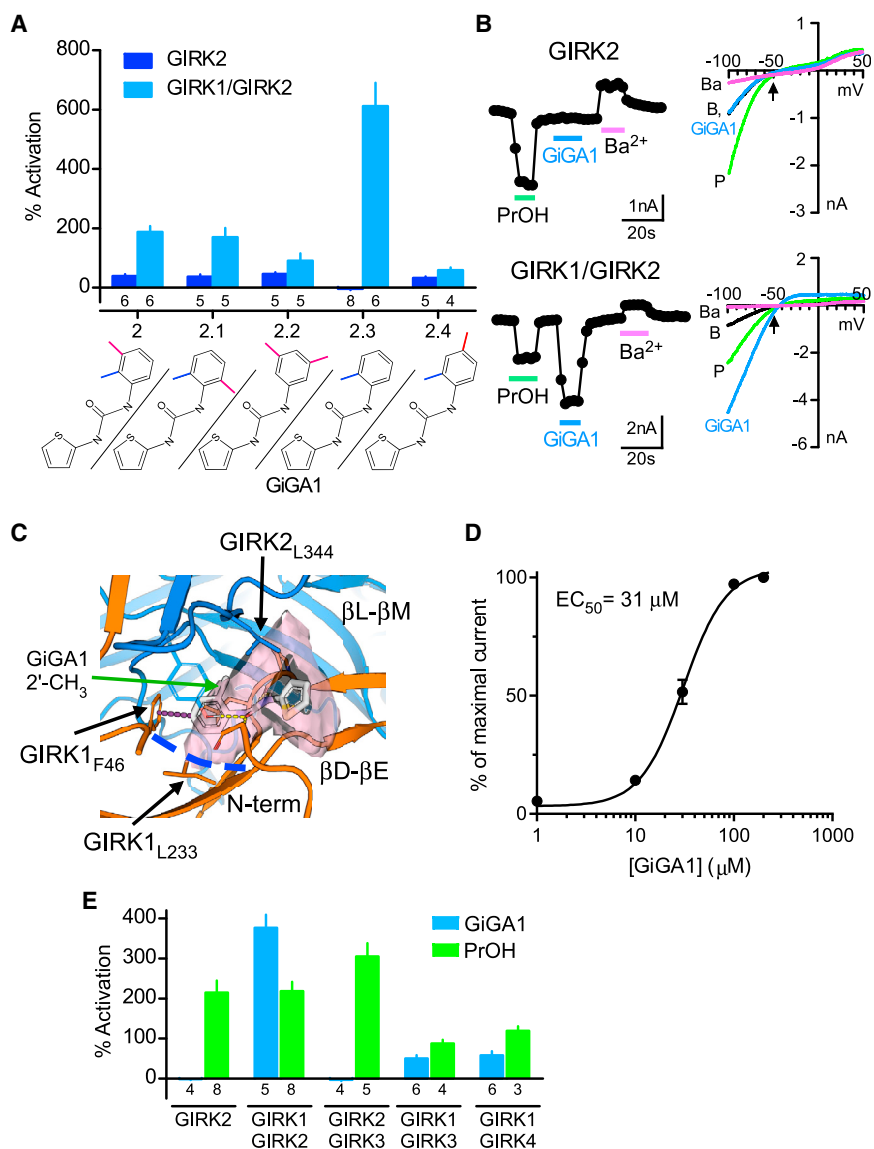


Figure 2. Characterization of a GIRK1-Specific Activator, GiGA1

(A) Bar graph shows the mean percentage of activation responses for GIRK2 and GIRK1/GIRK2 channels to compound 2 and its analogs, varying the position or number of methyl groups on the phenyl ring (100 μM). The chemical structure for each compound is shown on the bottom. Currents are normalized to the Ba^{2+} -sensitive basal current. Compound 2.3 showed specificity for GIRK1/GIRK2 (called GiGA1). n is indicated on the graph. (B) Traces show the current response to PrOH (100 mM), GiGA1 (100 μM), and Ba^{2+} (1 mM) for GIRK2 (top trace) and GIRK1/GIRK2 channels (bottom trace). Current-voltage plots for GIRK2 channels (top) and GIRK1/GIRK2 channels (bottom) recorded in the absence (black) and presence of PrOH (green), GiGA1 (blue), and Ba^{2+} (magenta). The arrow indicates $E_{\text{K}} = -50$ mV, with 20 mM K_{out} .

(C) Predicted binding mode of GiGA1 (white sticks) to a model of the GIRK1/GIRK2 (orange and blue cartoons, respectively) alcohol pocket from IFD. The binding pocket is depicted as a pink surface; the upper boundary of the pocket is limited by $\text{GIRK2}_{\text{L344}}$, and the lower boundary is marked by $\text{GIRK1}_{\text{L233}}$ (blue dashed line). *o*-methylphenyl moiety of GiGA1 is predicted to form π - π interactions with $\text{GIRK1}_{\text{F46}}$ (purple dashed line). Note the position in the pocket of 2' CH_3 on the phenyl ring of GiGA1.

(D) Dose-response fit with the Hill equation is shown for activation of GIRK1/GIRK2 channels by GiGA1 (n = 6 cells). $\text{EC}_{50} = 31$ μM and Hill coefficient = 2.0.

(E) Bar graph shows the mean change in percentage of activation for subtypes of GIRK channels to 25 μM GiGA1 (blue) and 100 mM PrOH (green). Note the specificity for GIRK1/GIRK2 subunits. n is indicated on the graphs. Error bars represent SEM on the graphs.

single mutation, the $\text{GIRK1}_{\text{L246W}}/\text{GIRK2}_{\text{L257W}}$ double mutation significantly reduced both PrOH- and GiGA1-activated currents (Figures 3D and 3E), suggesting involvement of all four alcohol pockets.

A GIRK1-selective activator, ML297, was identified through HTS, and its mechanism has been characterized (Kaufmann et al., 2013; Wydeven et al., 2014). Two unique amino acids, Phe137 and Asp173, located within the gating region of GIRK1 are necessary and sufficient to determine the specificity and action of ML297 (Wydeven et al., 2014) (Figure 4A). Because GiGA1-induced channel activity is also specific to GIRK1, we tested whether GiGA1 shares a similar mechanism of action with ML297. We examined the effect of $\text{GIRK1}_{\text{F137S}}$ (FS) and $\text{GIRK1}_{\text{D173N}}$ (DN) mutations, and as shown previously (Wydeven et al., 2014), each mutation significantly reduced the activation by ML297. By contrast, neither mutation in GIRK1 abolished the GiGA1-induced current (Figures 4B–4E). In addition to a

different site of action, the kinetics of the GiGA1- and ML297-induced currents are different. GiGA1 has a rapid deactivation rate, comparable to that of alcohol modulation of GIRK channels, whereas the off rate of ML297 is significantly slower (Figure S2A). We also tested the effect of Ba^{2+} to inhibit GiGA1 activation of GIRK1/GIRK2 by co-application of GiGA1 and Ba^{2+} (Figure S2B). Ba^{2+} blocked GIRK1/GIRK2 currents to the same extent and did not affect the reversal of GiGA1 activation.

We therefore focused on the alcohol pockets of GIRK1 and GIRK2 subunits (see sequence alignment, Figure S1) to further investigate the preferential activation of GIRK1/GIRK2 heterotetramers by GiGA1 (Figure 2). To identify key amino acids in the pocket that determine specificity, we first evaluated the effect of a series of mutations in the GIRK1 subunit. The alcohol pocket is composed of the N terminus and βD - βE loop from one subunit and βL - βM loop from the adjacent subunit and is therefore located at the interface of two adjoining subunits; thus, there

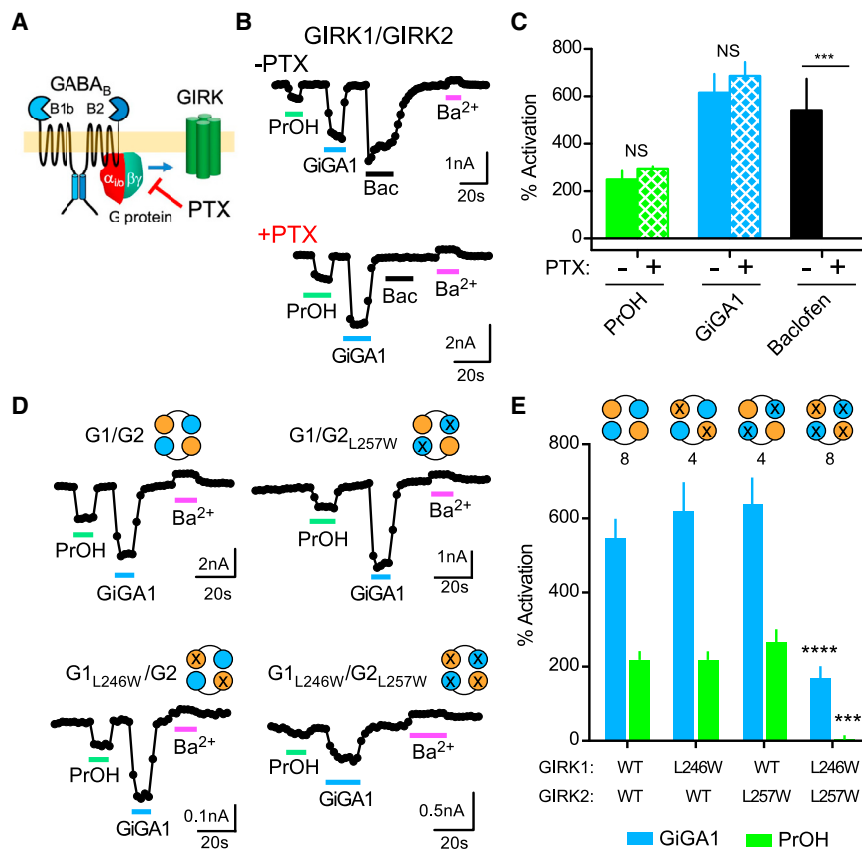


Figure 3. GiGA1 Activates GIRK1/GIRK2 Channels through an Alcohol Pocket in a G-Protein-Independent Manner

(A) Cartoon shows activation of the GIRK channel via the G-protein-dependent pathway, which is blocked by PTX. (B) Traces show the current response to PrOH (100 mM), GiGA1 (100 μ M), baclofen (100 μ M), and Ba^{2+} (1 mM) in HEK cells transfected with cDNA for $GABA_{B1b/B2}$ receptors and GIRK1/GIRK2c tandem dimer with or without the PTX S1 subunit. (C) Bar graph shows the mean change in percentage of activation for GIRK1/GIRK2 channels with PrOH (green), GiGA1 (blue), or baclofen (black) in the absence or presence of the PTX S1 subunit. *** $p = 0.0006$; $F(2, 5) = 25.52$ (baclofen \times PTX); mixed-effects model (restricted maximum likelihood [REML]) with Bonferroni post hoc ($n = 4$ (-PTX), 5 (+PTX)). (D) Traces for the WT GIRK1/GIRK2 channel and the indicated alcohol pocket mutation (GIRK1_{L246W}/GIRK2_{L257W}) (Aryal et al., 2009) in response to PrOH (100 mM), GiGA1 (100 μ M), and Ba^{2+} (1 mM). The schematic indicates the subunit that has a mutation; the orange circle is GIRK1, and the cyan circle is GIRK2. (E) Bar graph shows the mean percentage of activation response to GiGA1 and PrOH. *** $p = 0.0004$, **** $p < 0.0001$ versus GIRK1/GIRK2 WT; two-way repeated-measures ANOVA with Dunnett's multiple comparison test ($F(3, 20) = 5.298$; $p = 0.0075$ activator \times mutation). n is indicated on the graph. Error bars represent SEM on the graphs.

are two different pairs of alcohol pockets in GIRK1/GIRK2 heterotetramers. The features of GIRK1 that support GiGA1-selective activation of GIRK1/GIRK2 channels could be distributed in all four pockets on different regions of GIRK1 and GIRK2 (Figure 5A). By comparing protein sequences of GIRK1 and GIRK2 subunit within the alcohol pocket, we selected amino acids that are different between GIRK1 and GIRK2, and could potentially affect binding of GiGA1 (Figure S1). To test this, we examined the effect of individually replacing five amino acids of GIRK1 that face the pocket with the corresponding amino acid in GIRK2. To quantify effects of mutations on GiGA1 activation, we calculated the GiGA1-induced current as the percentage of the ML297-induced response (GiGA1/ML297), which is not expected to change with the mutation. F46Y, C230A, L233I, E250D, and F338Y mutations in GIRK1 did not alter the activation by GiGA1 (% normalized activation), in contrast to the GIRK1_{L246W}/GIRK2_{L257W} double mutation in the alcohol pocket (Figure S3).

To identify other amino acids near the alcohol pocket, we generated a structural model of the GIRK1/GIRK2 alcohol pocket (see STAR Methods) (Figure 2C). One unique pair of amino acids was ideally positioned to potentially alter the alcohol pocket: Arg43 in GIRK1 and Asp346 in GIRK2. Arg43 in GIRK1 is localized outside of the alcohol pocket but could stabilize the pocket by forming a salt bridge with Asp346 in GIRK2. Mutation GIRK1_{R43I} significantly decreased the % normalized GiGA1-activated current, compared with WT channels (Figures 5B, 5C, and

5F). An alanine substitution produced a similar decrease in the % normalized GiGA1-activated current. We next examined an Ala or Ile substitution at GIRK2_{D346}. Interestingly, GIRK2_{D346A}, but not GIRK2_{D346I}, reduced % normalized GiGA1 activation (Figures 5D and 5F). To probe whether a salt bridge was essential, we examined the effect of charge reversal at Asp346. GIRK2_{D346K} was indistinguishable from that of WT (Figure 5F). Thus, the side-chain length, and not the charge, appeared to be important for conferring specificity of GiGA1 activation of GIRK1/GIRK2 channels. Lastly, we examined the effect of mutating all four pockets in the heterotetramers. The double-mutant GIRK1_{R43I}/GIRK2_{D346A} exhibited a statistically smaller % normalized GiGA1-activated current, compared with each of the single mutations (GIRK1_{R43I} or GIRK2_{D346A}) (Figures 5E and 5F). To validate that ML297 currents were not altered by the mutations, we analyzed current density for each of the mutants; only one of six mutants (D346I) significantly reduced ML297 current (Figure S6).

To gain insights into the effect of the GIRK1_{R43I}/GIRK2_{D346A} mutations on GiGA1 activation of the GIRK1/GIRK2 heterotetramer, we used Gaussian accelerated molecular dynamics (GaMD) simulations (see STAR Methods) that can assess the secondary structure elements of the residues lining the alcohol pocket. We observed that both GIRK1_{R43I} and GIRK2_{D346A} single mutations and the GIRK1_{R43I}/GIRK2_{D346A} double mutation have little impact on the secondary structure of the residue in the alcohol pocket, GIRK2_{L342} (Figure S4). However, these

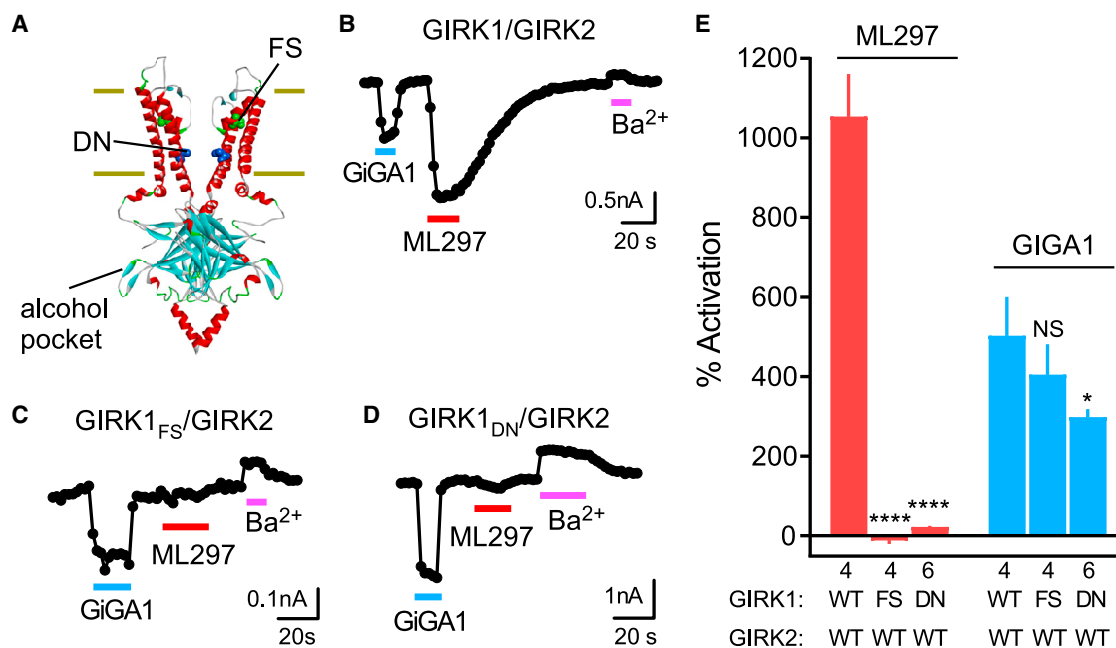


Figure 4. GiGA1 Activates GIRK1/GIRK2 Channels through a Different Mechanism from ML297

(A) Structural model of GIRK2 (PDB: 4KFM) shows the alcohol pocket and location of homologous amino acids in GIRK1 implicated previously in ML297 activation (FS (green), GIRK1_{F137} to ~GIRK2_{S148}; DN (blue), GIRK1_{D173} to ~GIRK2_{N184}). (B–D) Traces show the current response of the WT GIRK1/GIRK2 (B), GIRK1_{FS}/GIRK2 (C), and GIRK1_{DN}/GIRK2 (D) channels to GiGA1 (100 μ M), ML297 (10 μ M), and Ba²⁺ (1 mM). Both mutants abolished the ML297 response, but not the activation with GiGA1. (E) Bar graph shows the mean percentage of activation with GiGA1 and ML297. ****p < 0.0001, *p = 0.0374 versus GIRK1/GIRK2 WT; two-way repeated-measures ANOVA with Dunnett’s multiple comparison test (F(2, 11) = 106.3; p < 0.0001; activator \times mutation). n is indicated on the graph. Error bars represent SEM on the graph.

mutations perturbed each other’s secondary structure (Figure S4), as well as that of GIRK2_{L344} (Figure S5), a residue implicated in G β γ activation (Figures 1B and 2C). Thus, the combined effect of GIRK1_{R43I}/GIRK2_{D346A} mutations could alter the structure of the β L- β M loop, which forms one side of the alcohol pocket, or access to the pocket, and could be important for modulating GiGA1 activation of GIRK1/GIRK2 heterotetramers.

Role of GiGA1 on Ex Vivo Hippocampal Neurons

To investigate whether GiGA1 could activate natively expressed GIRK channels, we examined the effect of GiGA1 on GIRK currents in hippocampal CA1 pyramidal neurons, which express mostly GIRK1/GIRK2 heterotetramers (Liao et al., 1996; Leaney, 2003). In acutely prepared hippocampal slices, we found that a saturating concentration of baclofen (300 μ M) induced an outward current of \sim 120 pA and was selectively reversed with the GABA_B receptor (GABA_BR) antagonist CGP55845 (5 μ M). We then bath applied GiGA1 (100 μ M), which also activated an outward current of \sim 120 pA and was sensitive to inhibition with Ba²⁺ (Figures 6A and 6B). In contrast, there was no change in the voltage-gated outward K⁺ currents measured at 0 mV (Figure 6B). GABA_BR-activated GIRK currents have been shown previously to hyperpolarize resting potential and reduce neuronal excitability (Yamada et al., 1998). In current-clamp recordings, GiGA1 significantly hyperpolarized the RMP following

CGP55845 inhibition, to the same level as baclofen (Figure 6C). In addition, GiGA1 significantly suppressed the number of spikes induced by current injection in pyramidal neurons (Figures 6D and 6E).

Ba²⁺ is known to inhibit several types of K⁺ channels (Piasta et al., 2011). We therefore explored whether the GiGA1-activated current could be selectively reversed with a GIRK-selective inhibitor. Kuzhikandathil and Oxford, 2002 reported that the D1 receptor antagonist SCH23390 inhibits GIRK channels (Figure 6F). Similar to Ba²⁺, bath application of SCH23390 (30 μ M) inhibited GiGA1-induced outward current (Figures 6G and 6H). Importantly, there was good agreement between the amplitude of the GiGA1-induced current and that of the SCH23390-inhibited current (Figure 6H). Altogether, these results demonstrate that GiGA1 may control the excitability of a CA1 pyramidal neuron by activating GIRK1/GIRK2 channels.

Potential Protective Role of GiGA1 in Epilepsy

Because activation of GIRK channels in the brain is expected to reduce membrane excitability, and GIRK2 KO mice show spontaneous convulsions (Signorini et al., 1997), we asked whether GiGA1 possesses antiseizure properties in an *in vivo* epilepsy model. We induced acute epilepsy in mice by intraperitoneal (i.p.) injection of PTZ. PTZ is thought to generate tonic-clonic seizure by antagonizing GABA_A receptors (Shimada and Yamagata, 2018). We first determined that 60 mg/kg PTZ induced

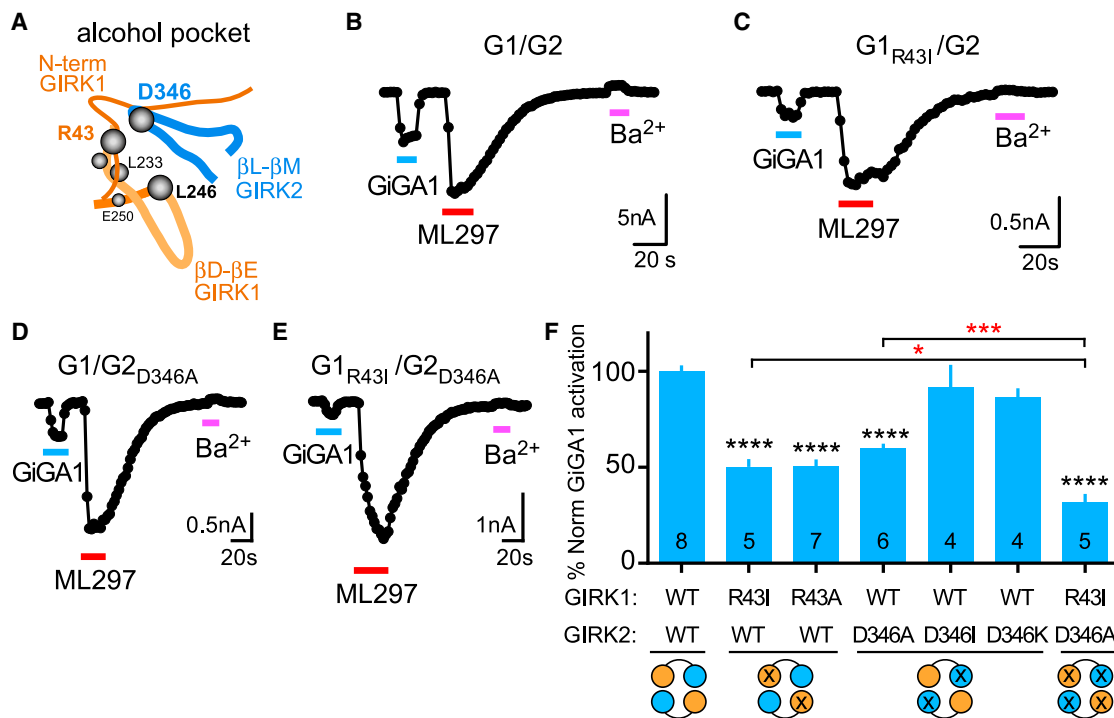


Figure 5. Identification of Amino Acids in GIRK1 that Contribute to GIRK1 Specificity of GiGA1

(A) Schematic depicts the alcohol pocket in one of the GIRK1/GIRK2 subunit interfaces, composed of the N-terminal domain and β D- β E loop from the GIRK1 subunit and β L- β M loop from the GIRK2 subunit. (B–E) Whole-cell patch-clamp recordings show the current response of WT G1/G2 (B), G1_{R43I}/G2 (C), G1/G2_{D346A} (D), and G1_{R43I}/G2_{D346A} (E) channels to GiGA1 (100 μ M), ML297 (10 μ M), and Ba²⁺ (1 mM). (F) Bar graph shows the mean percentage of GiGA1 activation normalized to ML297-induced currents and WT (see STAR Methods). ****p < 0.0001 versus GIRK1/GIRK2 WT, *p = 0.0385 GIRK1_{R43I}, ***p = 0.0006 GIRK2_{D346A} versus GIRK1_{R43I}/GIRK2_{D346A}; one-way ANOVA with Bonferroni's multiple comparison test (F(6, 32) = 30.96; p < 0.0001). n is indicated on the graph. Error bars represent SEM on the graph.

distinct stages of seizure intensity without being lethal. We also investigated the pharmacokinetic (PK) properties of GiGA1 *in vivo*. GiGA1 displayed a higher concentration in the brain sample than the plasma sample throughout and reached a maximum brain concentration at 15 min after injection, which decreased significantly after 1 h (Figures S7A–S7C). To test the potential antiseizure property, we first injected GiGA1 (20, 40, or 60 mg/kg), vehicle (Veh), or the positive control valproic acid (VPA) (200 mg/kg) and then waited 15–30 min before injecting PTZ to induce seizures (Figure 7A). Seizure scores were analyzed for 30 min based on the modified Racine score (Shimada and Yamagata, 2018), and the time in a score of 3 and above was used as the time in the tonic seizure. Two doses of GiGA1 (40 and 60 mg/kg) significantly lowered the seizure score and reduced the time in tonic seizure by ~80% (Figures 7B and 7C). We also observed some dose-dependent sedative effects of GiGA1 (Figure S7D).

DISCUSSION

In the present study, we used an integrated approach of identifying a GIRK1-specific activator through computational modeling and subsequent biochemical and physiological studies. We first developed a structural model of the putative

alcohol binding site in GIRK2, allowing us to investigate the mode of interaction between GIRK2 and alcohol, as well as conduct a virtual screen of numerous compounds in a short amount of time. The atomic resolution model of an alcohol-bound GIRK2 channel provided us essential insights into the alcohol pocket, suggesting a key hydrophobic effect near Leu257, as well as additional hydrogen bonds with the backbone amides of Lys52 and Pro256 (Aryal et al., 2009; Pegan et al., 2006). These proposed interactions likely contributed to the accuracy of our initial virtual screening. Although the virtual screening was based on the alcohol pocket in GIRK2, we identified compounds that modulate GIRK channels other than GIRK2 homotetramers. This outcome may seem surprising at first, but the alcohol pocket is composed of structural elements (part of the N terminus and β D- β E and β L- β M loops) that are highly conserved among the GIRK channels. For example, conserved Pro256 and Leu257 in GIRK2 (P245 and L246 in GIRK1) are predicted to interact with the recently discovered modulators. Notably, through chemical modification of the initial hit (compound 2), we were able to improve the specificity for GIRK1.

Our results revealed that GiGA1 has a distinct site of action on GIRK1/GIRK2 channels. Under physiological conditions, G β γ subunits dissociate from heterotrimeric G $\alpha_{i/o}$ β γ proteins upon GPCR activation and directly activate GIRK channels

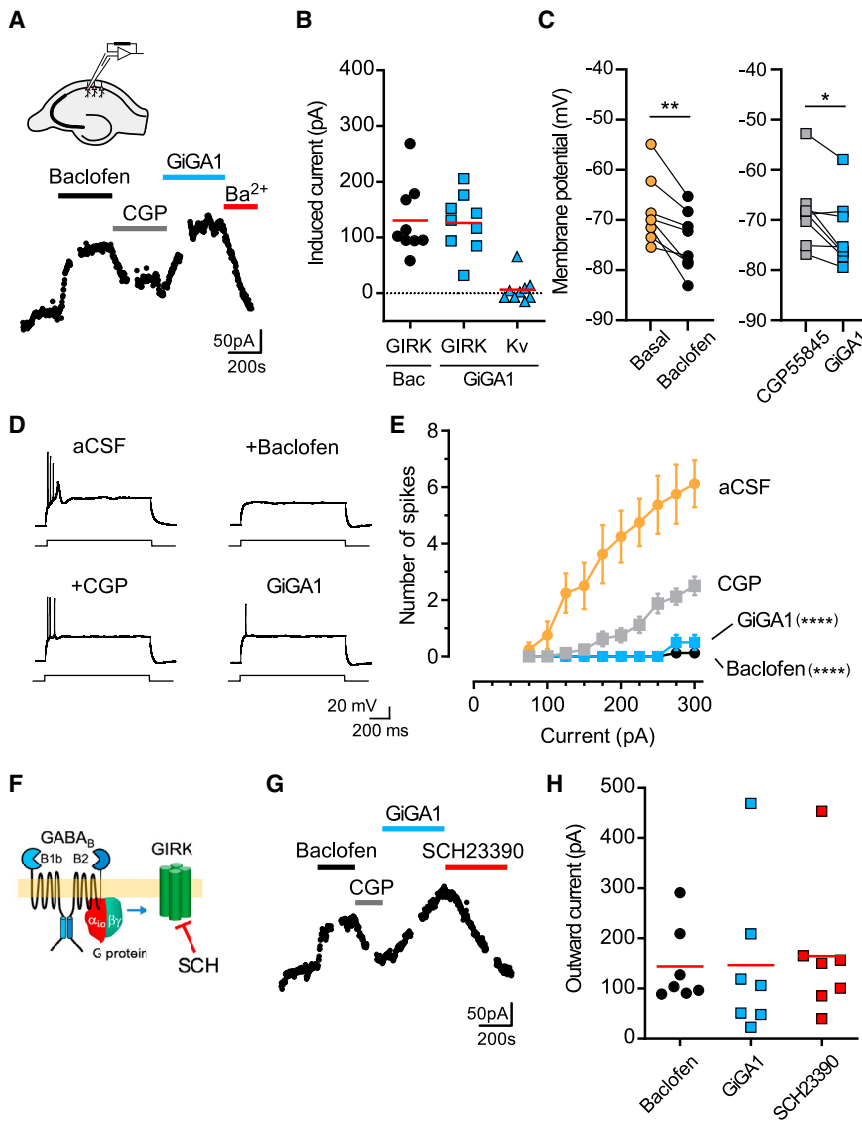


Figure 6. GiGA1 Induces GIRK Currents in Hippocampal CA1 Pyramidal Neurons

(A) Whole-cell patch-clamp recording from a hippocampal CA1 pyramidal neuron shows baclofen-induced (300 μ M) and GiGA1-induced (100 μ M) outward currents and inhibition by CGP55845 (5 μ M) and Ba^{2+} (1 mM), respectively. $V_H = -40$ mV. Schematic shows the hippocampal slice and placement of the recording pipette.

(B) Scatterplot shows baclofen- and GiGA1-induced GIRK currents measured at -40 mV, as well as outward voltage-gated K (Kv) currents measured at 0 mV. $n = 9$ cells. The ed bar indicates the mean.

(C) Plot shows the individual RMP ($I = 0$) in the absence (basal) and presence of baclofen (left graph) and the presence of CGP55845 followed by GiGA1 (right graph). $**p = 0.0028$ baclofen versus basal, $*p = 0.0182$ GiGA1 versus CGP55845; paired t test. $n = 8$ cells.

(D) Voltage traces show induced action potentials (+275 pA) in the presence of aCSF alone or with baclofen, CGP55845, or GiGA1.

(E) Input-output plots show the firing frequency increases as a function of current injections for artificial cerebrospinal fluid (aCSF) (basal) or CGP55845 (5 μ M) that are significantly suppressed by either baclofen (300 μ M) or GiGA1 (100 μ M), respectively. $****p < 0.0001$ for basal versus baclofen and CGP55845 versus GiGA1 ($n = 8$); two-way repeated-measures ANOVA with Tukey's multiple comparisons post hoc test for interaction between drug and current injection. Error bars represent SEM on the graph.

(F) Cartoon shows the inhibition of the GIRK channel by SCH23390 (Kuzhikandathil and Oxford, 2002; Montalbano et al., 2015).

(G) Whole-cell patch-clamp recording from the hippocampal CA1 pyramidal neuron shows baclofen-induced (300 μ M) and GiGA1-induced (100 μ M) outward currents and the response to CGP55845 (5 μ M) and a GIRK-selective inhibitor (SCH23390; 30 μ M), respectively.

(H) Scatterplot shows baclofen- and GiGA1-induced GIRK currents, as well as SCH23390-inhibited GIRK currents measured at -40 mV ($n = 7$ cells). The red bar indicates the mean (there is no significant difference).

(Huang et al., 1995; Inanobe et al., 1995; Reuveny et al., 1994). The critical region for $G\beta\gamma$ binding was mapped to residues localized near the alcohol pocket (Bodhinathan and Slesinger, 2014; Finley et al., 2004; Ivanina et al., 2003; Whorton and MacKinnon, 2013). We tested the involvement of $G\beta\gamma$ in GiGA1-mediated GIRK channel activation by co-expressing the PTX catalytic subunit. Like alcohol, GiGA1 activated GIRK channels in a G-protein-independent manner and was not affected by PTX expression. Another GIRK1-specific modulator, ML297, was identified through a thallium-based flux screening assay (Kaufmann et al., 2013). Similar to GiGA1, this compound activates GIRK channels in a G-protein-independent manner, with a preference for GIRK1-containing channels (Kaufmann et al., 2013). Molecular studies identified two amino acids in

the channel pore and membrane-spanning region of GIRK1 essential for its efficacy and selectivity (Wydeven et al., 2014). F137 is also implicated in the slow voltage-dependent gating property of the GIRK1 subunit (Kofuji et al., 1996). However, none of these sites appeared to be important for GiGA1-mediated activation. Furthermore, GiGA1 exhibits fast activation and deactivation properties that are similar to those of alcohol.

Does GiGA1 activate GIRK channels via the alcohol pocket? Mutation of a leucine shown previously to be important for alcohol activation (Aryal et al., 2009) significantly attenuated GiGA1-dependent activation, as well as decreasing ProH-dependent activation when all four leucines were mutated to Trp in both GIRK1 and GIRK2 subunits. Although these leucines are important for alcohol and GiGA1 activation, these mutations

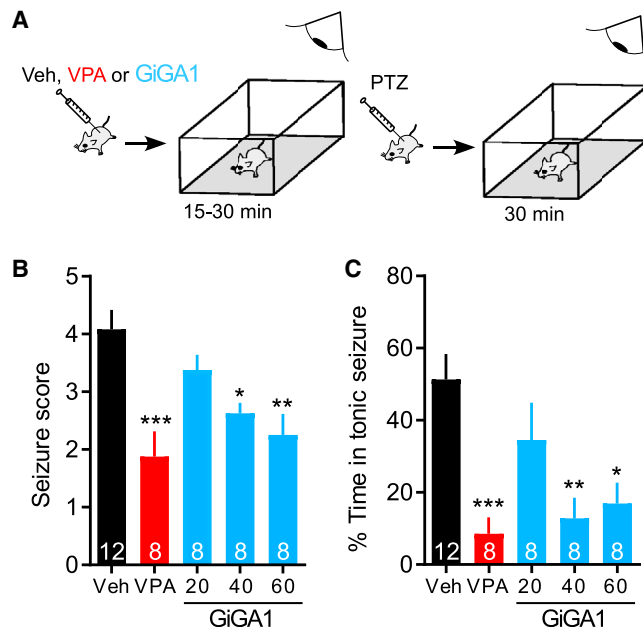


Figure 7. Anticonvulsive Effect of GiGA1 in the PTZ-Induced Epilepsy Model

(A) Schematic shows the time course of the experiment. WT C57BL/6J mice first received an i.p. injection of Veh, valproic acid (VPA, 200 mg/kg), or GiGA1 (20, 40, and 60 mg/kg), and then locomotor activity was monitored for 15–30 min. Mice then received an i.p. injection of PTZ (60 mg/kg) to induce acute seizures and were monitored for another 30 min.

(B) Bar graph shows mean seizure scores based on the modified Racine score (Shimada and Yamagata, 2018). * $p = 0.0278$, ** $p = 0.0026$, *** $p = 0.0002$ versus Veh; one-way ANOVA with Bonferroni's multiple comparison test ($F(4, 39) = 7.709$; $p = 0.0001$).

(C) Bar graph shows the mean percentage of time with seizure scores ≥ 3 . * $p = 0.0101$, ** $p = 0.0029$, *** $p = 0.0008$ versus Veh; one-way ANOVA with Bonferroni's multiple comparison test ($F(4, 39) = 7.067$; $p = 0.0002$).

n is indicated on the graphs. Error bars represent SEM on the graphs.

did not reveal the mechanism of specificity of GiGA1 activation of GIRK1/GIRK2 channels over GIRK2. Mutagenesis of other amino acids in the pocket that differed between GIRK1 and GIRK2 also did not produce changes in GiGA1 activation. We hypothesized that GiGA1 requires additional structural features, besides GIRK1_{L246}/GIRK2_{L257} in the pocket, to enable subunit specificity. We identified Arg43 in the N terminus of GIRK1 and Asp346 in the C-terminal β L- β M loop of GIRK2 that contribute to the specificity of GiGA1 activation of GIRK1/GIRK2 channels. Although these two residues carry opposite charges, and could therefore form a salt bridge, this interaction did not appear to be essential, because substituting Asp346 with the positively charged Lys did not alter GiGA1-dependent activation. The molecular dynamics simulations revealed that mutagenesis of either of these residues affects the secondary structure of each residue. In addition, mutation of these two residues appears to propagate to a residue within the pocket, GIRK2_{L344}. These findings suggest that the mutations allosterically alter the local secondary structure of the β L- β M loop, interfering with the proper binding of GiGA1 to the alcohol pocket, although we cannot rule out an additional site of action for GiGA1.

Altogether, these observations support the conclusion that GiGA1 is a GIRK1-specific modulator that may activate GIRK1/GIRK2 channels via the alcohol binding pocket. However, the precise binding mechanism of GiGA1 to GIRK1/GIRK2 channels should be explored by additional structural studies. One notable advantage over alcohol is the higher potency and saturating response of GiGA1, which is difficult to show with alcohols (Bodhinathan and Slesinger, 2014). The fast deactivation kinetics could be beneficial when an acute adjustment in channel activity is required; a slow off rate might result in undesirable excess activation of GIRK channels. GiGA1 showed good aqueous solubility (34 μ g/mL) at pH 7.4. *In vivo* PK studies, GiGA1 also produced a maximum brain-to-plasma ratio of 1.91 ± 0.86 when administered systemically (i.p.) to mice, which is an improvement over ML297 (0.2) (Kaufmann et al., 2013). Thus, GiGA1 could be evaluated for functional effects *in vivo*.

Previous studies implicated GIRK channels in controlling excitability and preventing seizures. GIRK2 KO mice showed spontaneous convulsions, as well as increased vulnerability to GABA_A receptor antagonist-induced seizures (Signorini et al., 1997). Similarly, GIRK2^{-/-}/GIRK3^{-/-} KO mice developed spontaneous and lethal seizures (Torrecilla et al., 2002). Furthermore, downregulation of GIRK channel function and expression occurs following neuronal injury during prolonged seizures (Baculis et al., 2017). Seizure induction and increased severity in these studies may be explained by the overall reduction of GIRK channel function, leading to hyperexcitability in many regions in the brain. Conversely, augmentation of GIRK channel activity in an epilepsy model may exert a protective effect, especially if focused on GIRK1/GIRK2 channels, the predominant form in the brain (Liao et al., 1996). In the current study, we show that GiGA1 preferentially activates GIRK1/GIRK2 channels, as well as those channels natively expressed in hippocampal pyramidal neurons (Koyrakh et al., 2005; Luján and Aguado, 2015). Studies of temporal lobe epilepsy have reported the involvement of the hippocampus and suggest that the hippocampus plays an essential role in epilepsy occurring and spreading (McIntyre and Racine, 1986; Diehl et al., 2004; Cascino, 2005). Accordingly, systemic administration of GiGA1 significantly reduced seizure severity and frequency of tonic seizures. These effects were comparable to the antiseizure effects of VPA, a commonly used antiepileptic drug (Pellock, 1994). Notably, increased self-grooming was seen in VPA-treated mice, but not in GiGA1-treated mice, which may reflect the actions of VPA on glutamatergic transmission in the prefrontal cortex (PFC) (Mehta et al., 2011). However, GiGA1 did show a dose-dependent sedative effect, although this outcome was not unexpected because GIRK-channel-deficient mice demonstrate a higher level of locomotion compared with WT (Morgan et al., 2003; Labouèbe et al., 2007; Arora et al., 2010) and baclofen, which partly targets the GABA_BR-GIRK signaling pathway and produces sedation (Gray et al., 1987; Ong and Kerr, 2005; Li et al., 2013). Lastly, alcohol is a sedative (Hendler et al., 2013). Future optimization of GiGA1 may mitigate some of these side effects *in vivo*.

In addition to an antiepileptic effect of GiGA1, selective activation of GIRK1/GIRK2 channels could be useful for treating other brain disorders, including alcohol use disorder (AUD) and

intractable pain. Alcohol affects multiple signaling pathways in the brain (Abraham et al., 2017). Systemic administration of baclofen significantly reduced alcohol intake in a binge-drinking mouse model (Moore et al., 2007). In alcohol-addicted rats, the acute treatment of baclofen blocked the increase of alcohol intake after alcohol deprivation (Colombo et al., 2003, 2006). In humans, several randomized controlled trials have demonstrated beneficial effects of baclofen in AUD (Addolorato et al., 2002, 2007; Müller et al., 2015; Morley et al., 2018). Furthermore, conditioning mechanisms, especially hippocampus-related ones, have been shown to play major roles in alcohol addiction (Kutlu and Gould, 2016). Because the major type of GIRK channels in the hippocampus is GIRK1/GIRK2, application of GiGA1 might prevent neuronal plasticity that is associated with alcohol-dependent contextual learning (Valyear et al., 2017). GiGA1 or a variant could be effective at treating AUD.

GIRK channels are also implicated in drug-induced analgesia. Many of these drugs activate GIRK channels either directly or through a G-protein-dependent pathway, including ethanol, baclofen, and opioids (Ikeda et al., 2000; Blednov et al., 2003). Lack of acute ethanol-induced analgesia was first demonstrated in *weaver* mice, which carry a mutation in the GIRK2 subunit (Panttilä et al., 1995). A subsequent study has shown that deletion of GIRK2 in mice reduced the antinociceptive effects of some analgesic drugs (Mitrovic et al., 2003). In GIRK2^{-/-}/GIRK3^{-/-} KO mice, morphine analgesia potency decreased, but efficacy was preserved (Cruz et al., 2008). In humans, single-nucleotide polymorphisms (SNPs) in GIRK2 were associated with decreased opioid sensitivity (Nishizawa et al., 2014), and subjects with these SNPs required an increased dose of opioid analgesics after abdominal surgery (Nishizawa et al., 2009). Because GiGA1 directly activates the GIRK1/GIRK2 channel in a G-protein-independent manner, it may offer non-opioid therapy for producing analgesia. Furthermore, because GiGA1 does not activate GIRK2/GIRK3 channels, the predominant form in the VTA (Cruz et al., 2004), it is less likely to show reinforcing effects. In conclusion, pharmacologically targeting subsets of GIRK channels in the brain may afford new opportunities for developing advanced therapeutics for treating various human neurological disorders.

STAR★METHODS

Detailed methods are provided in the online version of this paper and include the following:

- KEY RESOURCES TABLE
- RESOURCE AVAILABILITY
 - Lead Contact
 - Materials Availability
 - Data and Code Availability
- EXPERIMENTAL MODEL AND SUBJECT DETAILS
 - Cultures of HEK293 cells
 - Mice
- METHOD DETAILS
 - Homology Modeling
 - Virtual Screening
 - Molecular Dynamics Simulation
 - Molecular Biology and Cell Culture

- HEK293T Electrophysiology
- *Ex Vivo* Slice Electrophysiology
- *In Vivo* Seizure Model
- Locomotor Activity Analysis
- *In vivo* Pharmacokinetics

● QUANTIFICATION AND STATISTICAL ANALYSIS

SUPPLEMENTAL INFORMATION

Supplemental Information can be found online at <https://doi.org/10.1016/j.celrep.2020.107770>.

ACKNOWLEDGMENTS

This work has been supported in part by National Institutes of Health (NIH) grants from the National Institute on Alcohol Abuse and Alcoholism, USA (R01AA018734) to P.A. Slesinger and from the National Institute of General Medical Sciences, USA (R01 GM108911) to A. Schlessinger. and P.M.-U.Ung. This work was supported in part through the computational resources and staff expertise provided by the Department of Scientific Computing at the Icahn School of Medicine at Mount Sinai and by the Intramural Research Program of the National Center for Advancing Translational Sciences (NCATS), NIH. The graphical abstract was created with [BioRender.com](https://www.biorender.com).

AUTHOR CONTRIBUTIONS

Y.Z., P.M.-U.U., I.W.G., A. Schlessinger, and P.A.S. helped create and design the experiments. P.M.-U.U., A. Schlessinger, and G.Z.-K. carried out computations. G.Z.-K., A.V.Z., N.J.M., A. Simeonov, G.R., and J.J.M. synthesized and provided small molecules, conducted PK experiments, and analyzed the data. Y.Z. carried out functional screening. Y.Z. and P.A.S. conducted electrophysiological data analyses. Y.Z. and P.A.S. wrote the manuscript. Y.Z., P.M.-U.U., G.Z.-K., A.V.Z., N.J.M., A. Simeonov, I.W.G., G.R., A. Schlessinger, J.J.M., and P.A.S. provided comments on the manuscript.

DECLARATION OF INTERESTS

A. Schlessinger is a co-founder of Alchemy.

Received: December 4, 2019

Revised: March 24, 2020

Accepted: May 22, 2020

Published: June 16, 2020

REFERENCES

- Abraham, K.P., Salinas, A.G., and Lovinger, D.M. (2017). Alcohol and the Brain: Neuronal Molecular Targets, Synapses, and Circuits. *Neuron* 96, 1223–1238.
- Addolorato, G., Caputo, F., Capristo, E., Domenicali, M., Bernardi, M., Janiri, L., Agabio, R., Colombo, G., Gessa, G.L., and Gasbarrini, G. (2002). Baclofen efficacy in reducing alcohol craving and intake: a preliminary double-blind randomized controlled study. *Alcohol Alcohol.* 37, 504–508.
- Addolorato, G., Leggio, L., Ferrulli, A., Cardone, S., Vonghia, L., Mirijello, A., Abenavoli, L., D'Angelo, C., Caputo, F., Zamboni, A., et al. (2007). Effectiveness and safety of baclofen for maintenance of alcohol abstinence in alcohol-dependent patients with liver cirrhosis: randomised, double-blind controlled study. *Lancet* 370, 1915–1922.
- Arora, D., Haluk, D.M., Kourrich, S., Pravetoni, M., Fernández-Alacid, L., Nicolau, J.C., Luján, R., and Wickman, K. (2010). Altered neurotransmission in the mesolimbic reward system of *Girk* mice. *J. Neurochem.* 114, 1487–1497.
- Aryal, P., Dvir, H., Choe, S., and Slesinger, P.A. (2009). A discrete alcohol pocket involved in GIRK channel activation. *Nat. Neurosci.* 12, 988–995.
- Baculis, B.C., Weiss, A.C., Pang, W., Jeong, H.G., Lee, J.H., Liu, D.C., Tsai, N.P., and Chung, H.J. (2017). Prolonged seizure activity causes caspase

- dependent cleavage and dysfunction of G-protein activated inwardly rectifying potassium channels. *Sci. Rep.* **7**, 12313.
- Best, T.K., Siarey, R.J., and Galdzicki, Z. (2007). Ts65Dn, a mouse model of Down syndrome, exhibits increased GABAB-induced potassium current. *J. Neurophysiol.* **97**, 892–900.
- Blednov, Y.A., Stoffel, M., Alva, H., and Harris, R.A. (2003). A pervasive mechanism for analgesia: activation of GIRK2 channels. *Proc. Natl. Acad. Sci. USA* **100**, 277–282.
- Bodhinathan, K., and Slesinger, P.A. (2013). Molecular mechanism underlying ethanol activation of G-protein-gated inwardly rectifying potassium channels. *Proc. Natl. Acad. Sci. USA* **110**, 18309–18314.
- Bodhinathan, K., and Slesinger, P.A. (2014). Alcohol modulation of G-protein-gated inwardly rectifying potassium channels: From binding to therapeutics. *Front. Physiol.* **5**, 76.
- Cascino, G.D. (2005). Temporal lobe epilepsy: more than hippocampal pathology. *Epilepsy Curr.* **5**, 187–189.
- Case, D.A., Cheatham, T.E., 3rd, Darden, T., Gohlke, H., Luo, R., Merz, K.M., Jr., Onufriev, A., Simmerling, C., Wang, B., and Woods, R.J. (2005). The Amber biomolecular simulation programs. *J. Comput. Chem.* **26**, 1668–1688.
- Colombo, G., Serra, S., Brunetti, G., Vacca, G., Carai, M.A., and Gessa, G.L. (2003). Suppression by baclofen of alcohol deprivation effect in Sardinian alcohol-preferring (sP) rats. *Drug Alcohol Depend.* **70**, 105–108.
- Colombo, G., Serra, S., Vacca, G., Carai, M.A., and Gessa, G.L. (2006). Baclofen-induced suppression of alcohol deprivation effect in Sardinian alcohol-preferring (sP) rats exposed to different alcohol concentrations. *Eur. J. Pharmacol.* **550**, 123–126.
- Cruz, H.G., Ivanova, T., Lunn, M.L., Stoffel, M., Slesinger, P.A., and Lüscher, C. (2004). Bi-directional effects of GABA(B) receptor agonists on the mesolimbic dopamine system. *Nat. Neurosci.* **7**, 153–159.
- Cruz, H.G., Berton, F., Sollini, M., Blanchet, C., Pravetoni, M., Wickman, K., and Lüscher, C. (2008). Absence and rescue of morphine withdrawal in GIRK/Kir3 knock-out mice. *J. Neurosci.* **28**, 4069–4077.
- Darden, T., York, D., and Pedersen, L. (1993). Particle mesh Ewald: An N-log(N) method for Ewald sums in large systems. *J. Chem. Phys.* **98**, 10089.
- Dascal, N. (1997). Signalling via the G protein-activated K⁺ channels. *Cell. Signal.* **9**, 551–573.
- Diehl, B., Najm, I., LaPresto, E., Prayson, R., Ruggieri, P., Mohamed, A., Ying, Z., Lieber, M., Babb, T., Bingaman, W., and Lüders, H.O. (2004). Temporal lobe volumes in patients with hippocampal sclerosis with or without cortical dysplasia. *Neurology* **62**, 1729–1735.
- Finley, M., Arrabit, C., Fowler, C., Suen, K.F., and Slesinger, P.A. (2004). β L- β M loop in the C-terminal domain of G protein-activated inwardly rectifying K⁺ channels is important for G β γ subunit activation. *J. Physiol.* **555**, 643–657.
- Glaaser, Ian, and Slesinger, Paul A. (2017). Dual activation of neuronal G protein-gated inwardly rectifying potassium (GIRK) channels by cholesterol and alcohol. *Scientific Reports* **7**, 4592.
- Goldenberg, M.M. (2010). Overview of drugs used for epilepsy and seizures: etiology, diagnosis, and treatment. *P&T* **35**, 392–415.
- Gray, J.A., Goodwin, G.M., Heal, D.J., and Green, A.R. (1987). Hypothermia induced by baclofen, a possible index of GABAB receptor function in mice, is enhanced by antidepressant drugs and ECS. *Br. J. Pharmacol.* **92**, 863–870.
- Harashima, C., Jacobowitz, D.M., Witt, J., Borke, R.C., Best, T.K., Siarey, R.J., and Galdzicki, Z. (2006). Abnormal expression of the G-protein-activated inwardly rectifying potassium channel 2 (GIRK2) in hippocampus, frontal cortex, and substantia nigra of Ts65Dn mouse: a model of Down syndrome. *J. Comp. Neurol.* **494**, 815–833.
- Harder, E., Damm, W., Maple, J., Wu, C., Reboul, M., Xiang, J.Y., Wang, L., Lupyan, D., Dahlgren, M.K., Knight, J.L., et al. (2016). OPLS3: A Force Field Providing Broad Coverage of Drug-like Small Molecules and Proteins. *J. Chem. Theory Comput.* **12**, 281–296.
- Hendler, R.A., Ramchandani, V.A., Gilman, J., and Hommer, D.W. (2013). Stimulant and sedative effects of alcohol. *Curr. Top. Behav. Neurosci.* **13**, 489–509.
- Hibino, H., Inanobe, A., Furutani, K., Murakami, S., Findlay, I., and Kurachi, Y. (2010). Inwardly rectifying potassium channels: their structure, function, and physiological roles. *Physiol. Rev.* **90**, 291–366.
- Horvath, G.A., Zhao, Y., Tarailo-Graovac, M., Boelman, C., Gill, H., Shyr, C., Lee, J., Blydt-Hansen, I., Drögemöller, B.I., Moreland, J., et al. (2018). Gain-of-function KCNJ6 Mutation in a Severe Hyperkinetic Movement Disorder Phenotype. *Neuroscience* **384**, 152–164.
- Huang, C.L., Slesinger, P.A., Casey, P.J., Jan, Y.N., and Jan, L.Y. (1995). Evidence that direct binding of G β γ to the GIRK1 G protein-gated inwardly rectifying K⁺ channel is important for channel activation. *Neuron* **15**, 1133–1143.
- Ikeda, K., Kobayashi, T., Kumanishi, T., Niki, H., and Yano, R. (2000). Involvement of G-protein-activated inwardly rectifying K (GIRK) channels in opioid-induced analgesia. *Neurosci. Res.* **38**, 113–116.
- Inanobe, A., Morishige, K.I., Takahashi, N., Ito, H., Yamada, M., Takumi, T., Nishina, H., Takahashi, K., Kanaho, Y., Katada, T., and Kurachi, Y. (1995). G β γ directly binds to the carboxyl terminus of the G protein-gated muscarinic K⁺ channel, GIRK1. *Biochem. Biophys. Res. Commun.* **212**, 1022–1028.
- Inanobe, A., Yoshimoto, Y., Horio, Y., Morishige, K.I., Hibino, H., Matsumoto, S., Tokunaga, Y., Maeda, T., Hata, Y., Takai, Y., and Kurachi, Y. (1999). Characterization of G-protein-gated K⁺ channels composed of Kir3.2 subunits in dopaminergic neurons of the substantia nigra. *J. Neurosci.* **19**, 1006–1017.
- Itoh, K., and Watanabe, M. (2009). Paradoxical facilitation of pentylentetrazole-induced convulsion susceptibility in mice lacking neuronal nitric oxide synthase. *Neuroscience* **159**, 735–743.
- Itoh, K., Watanabe, M., Yoshikawa, K., Kanaho, Y., Berliner, L.J., and Fujii, H. (2004). Magnetic resonance and biochemical studies during pentylentetrazole-kindling development: the relationship between nitric oxide, neuronal nitric oxide synthase and seizures. *Neuroscience* **129**, 757–766.
- Ivanina, T., Rishal, I., Varon, D., Müllner, C., Frohnes-Steinecke, B., Schreibmayer, W., Dessauer, C.W., and Dascal, N. (2003). Mapping the G β γ -binding sites in GIRK1 and GIRK2 subunits of the G protein-activated K⁺ channel. *J. Biol. Chem.* **278**, 29174–29183.
- Jorgensen, W.L., Chandrasekhar, J., and Madura, J.D. (1983). Comparison of simple potential functions for simulating liquid water. *J. Chem. Phys.* **79**, 926–935.
- Karschin, C., Dissmann, E., Stühmer, W., and Karschin, A. (1996). IRK(1-3) and GIRK(1-4) inwardly rectifying K⁺ channel mRNAs are differentially expressed in the adult rat brain. *J. Neurosci.* **16**, 3559–3570.
- Kaufmann, K., Romaine, I., Days, E., Pascual, C., Malik, A., Yang, L., Zou, B., Du, Y., Sliwoski, G., Morrison, R.D., et al. (2013). ML297 (VU0456810), the first potent and selective activator of the GIRK potassium channel, displays anti-epileptic properties in mice. *ACS Chem. Neurosci.* **4**, 1278–1286.
- Kobayashi, T., Ikeda, K., Ichikawa, T., Abe, S., Togashi, S., and Kumanishi, T. (1995). Molecular cloning of a mouse G-protein-activated K⁺ channel (mGIRK1) and distinct distributions of three GIRK (GIRK1, 2 and 3) mRNAs in mouse brain. *Biochem. Biophys. Res. Commun.* **208**, 1166–1173.
- Kobayashi, T., Ikeda, K., Kojima, H., Niki, H., Yano, R., Yoshioka, T., and Kumanishi, T. (1999). Ethanol opens G-protein-activated inwardly rectifying K⁺ channels. *Nat. Neurosci.* **2**, 1091–1097.
- Kofuji, P., Doupnik, C.A., Davidson, N., and Lester, H.A. (1996). A unique P-region residue is required for slow voltage-dependent gating of a G protein-activated inward rectifier K⁺ channel expressed in *Xenopus oocytes*. *J. Physiol.* **490**, 633–645.
- Koyrakh, L., Luján, R., Colón, J., Karschin, C., Kurachi, Y., Karschin, A., and Wickman, K. (2005). Molecular and cellular diversity of neuronal G-protein-gated potassium channels. *J. Neurosci.* **25**, 11468–11478.
- Kutlu, M.G., and Gould, T.J. (2016). Effects of drugs of abuse on hippocampal plasticity and hippocampus-dependent learning and memory: contributions to development and maintenance of addiction. *Learn. Mem.* **23**, 515–533.

- Kuzhikandathil, E.V., and Oxford, G.S. (2002). Classic D1 dopamine receptor antagonist R-(+)-7-chloro-8-hydroxy-3-methyl-1-phenyl-2,3,4,5-tetrahydro-1H-3-benzazepine hydrochloride (SCH23390) directly inhibits G protein-coupled inwardly rectifying potassium channels. *Mol. Pharmacol.* **62**, 119–126.
- Labouèbe, G., Lomazzi, M., Cruz, H.G., Creton, C., Luján, R., Li, M., Yanagawa, Y., Obata, K., Watanabe, M., Wickman, K., et al. (2007). RGS2 modulates coupling between GABAB receptors and GIRK channels in dopamine neurons of the ventral tegmental area. *Nat. Neurosci.* **10**, 1559–1568.
- Leaney, J.L. (2003). Contribution of Kir3.1, Kir3.2A and Kir3.2C subunits to native G protein-gated inwardly rectifying potassium currents in cultured hippocampal neurons. *Eur. J. Neurosci.* **18**, 2110–2118.
- Lee, T.S., Cerutti, D.S., Mermelstein, D., Lin, C., LeGrand, S., Giese, T.J., Roitberg, A., Case, D.A., Walker, R.C., and York, D.M. (2018). GPU-Accelerated Molecular Dynamics and Free Energy Methods in Amber18: Performance Enhancements and New Features. *J. Chem. Inf. Model.* **58**, 2043–2050.
- Lesage, F., Guillemare, E., Fink, M., Duprat, F., Heurteaux, C., Fosset, M., Romey, G., Barhanin, J., and Lazdunski, M. (1995). Molecular properties of neuronal G-protein-activated inwardly rectifying K⁺ channels. *J. Biol. Chem.* **270**, 28660–28667.
- Lewohl, J.M., Wilson, W.R., Mayfield, R.D., Brozowski, S.J., Morrisett, R.A., and Harris, R.A. (1999). G-protein-coupled inwardly rectifying potassium channels are targets of alcohol action. *Nat. Neurosci.* **2**, 1084–1090.
- Li, X., Risbrough, V.B., Cates-Gatto, C., Kaczanowska, K., Finn, M.G., Roberts, A.J., and Markou, A. (2013). Comparison of the effects of the GABAB receptor positive modulator BHF177 and the GABAB receptor agonist baclofen on anxiety-like behavior, learning, and memory in mice. *Neuropharmacology* **70**, 156–167.
- Liao, Y.J., Jan, Y.N., and Jan, L.Y. (1996). Heteromultimerization of G-protein-gated inwardly rectifying K⁺ channel proteins GIRK1 and GIRK2 and their altered expression in weaver brain. *J. Neurosci.* **16**, 7137–7150.
- Luján, R., and Aguado, C. (2015). Localization and Targeting of GIRK Channels in Mammalian Central Neurons. *Int. Rev. Neurobiol.* **123**, 161–200.
- Lüscher, C., and Slesinger, P.A. (2010). Emerging roles for G protein-gated inwardly rectifying potassium (GIRK) channels in health and disease. *Nat. Rev. Neurosci.* **11**, 301–315.
- Lüscher, C., Jan, L.Y., Stoffel, M., Malenka, R.C., and Nicoll, R.A. (1997). G protein-coupled inwardly rectifying K⁺ channels (GIRKs) mediate postsynaptic but not presynaptic transmitter actions in hippocampal neurons. *Neuron* **19**, 687–695.
- Masotti, A., Uva, P., Davis-Keppen, L., Basel-Vanagaite, L., Cohen, L., Pisaneschi, E., Celluzzi, A., Bencivenga, P., Fang, M., Tian, M., et al. (2015). Keppen-Lubinsky syndrome is caused by mutations in the inwardly rectifying K⁺ channel encoded by KCNJ6. *Am. J. Hum. Genet.* **96**, 295–300.
- McIntyre, D.C., and Racine, R.J. (1986). Kindling mechanisms: current progress on an experimental epilepsy model. *Prog. Neurobiol.* **27**, 1–12.
- Mehta, M.V., Gandal, M.J., and Siegel, S.J. (2011). mGluR5-antagonist mediated reversal of elevated stereotyped, repetitive behaviors in the VPA model of autism. *PLoS ONE* **6**, e26077.
- Miao, Y., Feher, V.A., and McCammon, J.A. (2015). Gaussian Accelerated Molecular Dynamics: Unconstrained Enhanced Sampling and Free Energy Calculation. *J. Chem. Theory Comput.* **11**, 3584–3595.
- Mitrovic, I., Margeta-Mitrovic, M., Bader, S., Stoffel, M., Jan, L.Y., and Basbaum, A.I. (2003). Contribution of GIRK2-mediated postsynaptic signaling to opiate and α 2-adrenergic analgesia and analgesic sex differences. *Proc. Natl. Acad. Sci. USA* **100**, 271–276.
- Montalbano, A., Corradetti, R., and Mlinar, B. (2015). Pharmacological characterization of 5-HT1A autoreceptor-coupled GIRK channels in rat dorsal raphe 5-HT neurons. *PLoS ONE* **10**, e0140369.
- Moore, E.M., Serio, K.M., Goldfarb, K.J., Stepanovska, S., Linsenbardt, D.N., and Boehm, S.L., 2nd. (2007). GABAergic modulation of binge-like ethanol intake in C57BL/6J mice. *Pharmacol. Biochem. Behav.* **88**, 105–113.
- Morgan, A.D., Carroll, M.E., Loth, A.K., Stoffel, M., and Wickman, K. (2003). Decreased cocaine self-administration in Kir3 potassium channel subunit knockout mice. *Neuropsychopharmacology* **28**, 932–938.
- Morley, K.C., Baillie, A., Fraser, I., Furneaux-Bate, A., Dore, G., Roberts, M., Abdalla, A., Phung, N., and Haber, P.S. (2018). Baclofen in the treatment of alcohol dependence with or without liver disease: multisite, randomised, double-blind, placebo-controlled trial. *Br. J. Psychiatry* **212**, 362–369.
- Müller, C.A., Geisel, O., Pelz, P., Higl, V., Krüger, J., Stickel, A., Beck, A., Wernecke, K.D., Hellweg, R., and Heinz, A. (2015). High-dose baclofen for the treatment of alcohol dependence (BACLAD study): a randomized, placebo-controlled trial. *Eur. Neuropsychopharmacol.* **25**, 1167–1177.
- Nishizawa, D., Nagashima, M., Katoh, R., Satoh, Y., Tagami, M., Kasai, S., Ogai, Y., Han, W., Hasegawa, J., Shimoyama, N., Sora, I., Hayashida, M., and Ikeda, K. (2009). Association between KCNJ6 (GIRK2) gene polymorphisms and postoperative analgesic requirements after major abdominal surgery. *PLoS ONE* **4**, e7060.
- Nishizawa, D., Fukuda, K., Kasai, S., Ogai, Y., Hasegawa, J., Sato, N., Yamada, H., Tanioka, F., Sugimura, H., Hayashida, M., and Ikeda, K. (2014). Association between KCNJ6 (GIRK2) gene polymorphism rs2835859 and postoperative analgesia, pain sensitivity, and nicotine dependence. *J. Pharmacol. Sci.* **126**, 253–263.
- Ong, J., and Kerr, D.I.B. (2005). Clinical potential of GABAB receptor modulators. *CNS Drug Rev.* **11**, 317–334.
- Patil, N., Cox, D.R., Bhat, D., Faham, M., Myers, R.M., and Peterson, A.S. (1995). A potassium channel mutation in weaver mice implicates membrane excitability in granule cell differentiation. *Nat. Genet.* **11**, 126–129.
- Pegan, S., Arrabit, C., Slesinger, P.A., and Choe, S. (2006). Andersen's syndrome mutation effects on the structure and assembly of the cytoplasmic domains of Kir2.1. *Biochemistry* **45**, 8599–8606.
- Pellock, J.M. (1994). Standard approach to antiepileptic drug treatment in the United States. *Epilepsia* **35** (Suppl 4), S11–S18.
- Piasta, K.N., Theobald, D.L., and Miller, C. (2011). Potassium-selective block of barium permeation through single KcsA channels. *J. Gen. Physiol.* **138**, 421–436.
- Porter, L.L., and Rose, G.D. (2011). Redrawing the Ramachandran plot after inclusion of hydrogen-bonding constraints. *Proc. Natl. Acad. Sci. USA* **108**, 109–113.
- Racine, R.J. (1972). Modification of seizure activity by electrical stimulation. II. Motor seizure. *Electroencephalogr. Clin. Neurophysiol.* **32**, 281–294.
- Reeves, R.H., Irving, N.G., Moran, T.H., Wohn, A., Kitt, C., Sisodia, S.S., Schmidt, C., Bronson, R.T., and Davison, M.T. (1995). A mouse model for Down syndrome exhibits learning and behaviour deficits. *Nat. Genet.* **11**, 177–184.
- Reisine, T. (1990). Pertussis toxin in the analysis of receptor mechanisms. *Biochem. Pharmacol.* **39**, 1499–1504.
- Reuveny, E., Slesinger, P.A., Inglese, J., Morales, J.M., Iñiguez-Lluhi, J.A., Lefkowitz, R.J., Bourne, H.R., Jan, Y.N., and Jan, L.Y. (1994). Activation of the cloned muscarinic potassium channel by G protein $\beta\gamma$ subunits. *Nature* **370**, 143–146.
- Rifkin, R.A., Huyghe, D., Li, X., Parakala, M., Aisenberg, E., Moss, S.J., and Slesinger, P.A. (2018). GIRK currents in VTA dopamine neurons control the sensitivity of mice to cocaine-induced locomotor sensitization. *Proc. Natl. Acad. Sci. USA* **115**, E9479–E9488.
- Roe, D.R., and Cheatham, T.E., 3rd. (2013). PTRAJ and CPPTRAJ: Software for processing and analysis of molecular dynamics trajectory data. *J. Chem. Theory Comput.* **9**, 3084–3095.
- Ryckaert, J.P., Ciccotti, G., and Berendsen, H.J.C. (1977). Numerical integration of the cartesian equations of motion of a system with constraints: molecular dynamics of n-alkanes. *J. Comput. Phys.* **23**, 327–341.
- Šali, A., and Blundell, T.L. (1993). Comparative protein modelling by satisfaction of spatial restraints. *J. Mol. Biol.* **234**, 779–815.
- Schlessinger, A., Geier, E., Fan, H., Irwin, J.J., Shoichet, B.K., Giacomini, K.M., and Sali, A. (2011). Structure-based discovery of prescription drugs that

- interact with the norepinephrine transporter, NET. *Proc. Natl. Acad. Sci. USA* **108**, 15810–15815.
- Schrödinger. (2017a). Glide, version 2 (Schrödinger).
- Schrödinger. (2017b). LigPrep, version 2 (Schrödinger).
- Shimada, T., and Yamagata, K. (2018). Pentylentetrazole-induced kindling mouse model. *J. Vis. Exp.* **136**, 56573.
- Signorini, S., Liao, Y.J., Duncan, S.A., Jan, L.Y., and Stoffel, M. (1997). Normal cerebellar development but susceptibility to seizures in mice lacking G protein-coupled, inwardly rectifying K⁺ channel GIRK2. *Proc. Natl. Acad. Sci. USA* **94**, 923–927.
- Slesinger, P.A., Stoffel, M., Jan, Y.N., and Jan, L.Y. (1997). Defective γ -aminobutyric acid type B receptor-activated inwardly rectifying K⁺ currents in cerebellar granule cells isolated from weaver and Girk2 null mutant mice. *Proc. Natl. Acad. Sci. USA* **94**, 12210–12217.
- Sterling, T., and Irwin, J.J. (2015). ZINC 15—Ligand Discovery for Everyone. *J. Chem. Inf. Model.* **55**, 2324–2337.
- Surmeier, D.J., Mermelstein, P.G., and Goldowitz, D. (1996). The weaver mutation of GIRK2 results in a loss of inwardly rectifying K⁺ current in cerebellar granule cells. *Proc. Natl. Acad. Sci. USA* **93**, 11191–11195.
- Tanimoto, T.T. (1969). Classification by computers: a generalized pearson-yule contingency technique and its application to automatic classification. *Ann. N Y Acad. Sci.* **161**, 420–423.
- Ting, J.T., Lee, B.R., Chong, P., Soler-Llavina, G., Cobbs, C., Koch, C., Zeng, H., and Lein, E. (2018). Preparation of Acute Brain Slices Using an Optimized N-Methyl-D-glucamine Protective Recovery Method. *J. Vis. Exp.* **132**, 53825.
- Torrecilla, M., Marker, C.L., Cintora, S.C., Stoffel, M., Williams, J.T., and Wickman, K. (2002). G-protein-gated potassium channels containing Kir3.2 and Kir3.3 subunits mediate the acute inhibitory effects of opioids on locus ceruleus neurons. *J. Neurosci.* **22**, 4328–4334.
- Valyear, M.D., Villaruel, F.R., and Chaudhri, N. (2017). Alcohol-seeking and relapse: A focus on incentive salience and contextual conditioning. *Behav. Processes* **141**, 26–32.
- Whorton, M.R., and MacKinnon, R. (2011). Crystal structure of the mammalian GIRK2 K⁺ channel and gating regulation by G proteins, PIP2, and sodium. *Cell* **147**, 199–208.
- Whorton, M.R., and MacKinnon, R. (2013). X-ray structure of the mammalian GIRK2- $\beta\gamma$ G-protein complex. *Nature* **498**, 190–197.
- Wickman, K., Karschin, C., Karschin, A., Picciotto, M.R., and Clapham, D.E. (2000). Brain localization and behavioral impact of the G-protein-gated K⁺ channel subunit GIRK4. *J. Neurosci.* **20**, 5608–5615.
- Wydeven, N., Marron Fernandez de Velasco, E., Du, Y., Benneyworth, M.A., Hearing, M.C., Fischer, R.A., Thomas, M.J., Weaver, C.D., and Wickman, K. (2014). Mechanisms underlying the activation of G-protein-gated inwardly rectifying K⁺ (GIRK) channels by the novel anxiolytic drug, ML297. *Proc. Natl. Acad. Sci. USA* **111**, 10755–10760.
- Yamada, M., Inanobe, A., and Kurachi, Y. (1998). G protein regulation of potassium ion channels. *Pharmacol. Rev.* **50**, 723–760.

STAR★METHODS

KEY RESOURCES TABLE

REAGENT or RESOURCE	SOURCE	IDENTIFIER
Chemicals, Peptides, and Recombinant Proteins		
Baclofen	Sigma-Aldrich	Catalog #: B5399
ML297	Sigma-Aldrich	Catalog #: SML0836
SCH23390	Sigma-Aldrich	Catalog #: D054
CGP55845	Sigma-Aldrich	Catalog #: SML0594
1-Propanol	Sigma-Aldrich	Catalog #: 402893
Barium Chloride	Sigma-Aldrich	Catalog #: 342920
Valproic acid	Sigma-Aldrich	Catalog #: P4543
Pentylentetrazol	Sigma-Aldrich	Catalog #: P6500
Critical Commercial Assays		
QuikChange II XL	Agilent Technology	
Experimental Models: Cell Lines		
HEK293T cells	ATCC	Catalog #: CRL-3216
Experimental Models: Organisms/Strains		
C57BL6/J mice (male and female)	Jackson Labs	Wild-type
CD1 mice (male) used for <i>in vivo</i> pharmacokinetic (PK) studies	Pharmaron labs	https://www.pharmaron.com/
Oligonucleotides		
DNA primers for mutagenesis	This study	N/A
Recombinant DNA		
rat GIRK1_mouse GIRK2c dimer cDNA	Horvath et al., 2018	N/A
mouse GIRK2c cDNA	Horvath et al., 2018	N/A
rat GIRK1_mouse GIRK3 dimer cDNA	This study	N/A
mouse GIRK3 cDNA	Cruz et al., 2004	N/A
rat GIRK4 cDNA	Aryal et al., 2009	N/A
human GABA _{B1b} cDNA	Horvath et al., 2018	N/A
human GABA _{B2} cDNA	Horvath et al., 2018	N/A
PTX S1 cDNA	This study	N/A
Software and Algorithms		
Prism 7.0	Graphpad	RRID:SCR_002798
Schrödinger (2017a, 2017b) , LigPrep, Glide	Schrödinger	https://www.schrodinger.com/ ; RRID: SCR_014879
MODELLER v9.18	(Sali and Blundell, 1993)	salilab.org/modeller; RRID: SCR_008395
MOE 2014.0901, 2016	Chemical Computing Group	https://www.chemcomp.com/ ; RRID: SCR_014882
OEDocking 3.2.0.2, FRED, OMEGA	OpenEye	https://www.eyesopen.com/ ; RRID: SCR_014880
KNIME		https://www.knime.com/ ; RRID: SCR_006164
JChem Cartridge	ChemAxon	https://chemaxon.com/ ; RRID: SCR_004111
StarDrop	Optibrium	https://www.optibrium.com/stardrop/ ; RRID: SCR_014902
FIJI	ImageJ	http://fiji.sc/ ; RRID: SCR_002285
PyMOL		https://pymol.org/2/ ; RRID: SCR_000305

RESOURCE AVAILABILITY

Lead Contact

Further information and requests for resources and reagents should be directed to and will be fulfilled by the Lead Contact, Paul Slesinger (paul.slesinger@mssm.edu).

Materials Availability

Plasmids generated in this study are available from the lead contact upon request. Compounds disclosed in this study are freely available upon request to NCATS and completion of regular NIH procedures in the form of a material transfer agreement (MTA). NCATS repository holds limited amounts of compounds. Additional amounts can be acquired from commercial sources. This study did not generate new unique reagents.

Data and Code Availability

The published article includes all data generated or analyzed during this study. This study did not generate any unique code.

EXPERIMENTAL MODEL AND SUBJECT DETAILS

Cultures of HEK293 cells

Human Embryonic Kidney 293T (HEK293T) cells were cultured in Dulbecco's modified Eagle's medium (DMEM Sigma-Aldrich, St. Louis, MO, USA) supplemented with 10% (v/v) Fetal Bovine Serum (FBS), 100 U/ml penicillin, 100 µg/ml streptomycin and 1X Glutamax (ThermoFisher) in a humidified 37°C incubator with 5% CO₂. Cells were plated onto poly-D-lysine (100 µg/ml; SigmaAldrich) coated 12-mm glass coverslips in 24-well plates and transiently transfected with cDNA using Lipofectamine 2000 (ThermoFisher).

Mice

All animal experiments were performed in accordance with institutional guidelines and approved protocol at Icahn School of Medicine at Mount Sinai's Institutional Animal Care and Use Committee. For brain slice recordings, both male and female C57BL/6 mice (8–12 weeks; Jackson labs) were used. For *in vivo* seizure study and the locomotor activity analysis, male C57BL/6 mice (3–4 months old, approximately 30 g; Jackson labs) were used. *In vivo* mouse pharmacokinetic (PK) studies were performed by Pharmaron Inc, using male CD1 mice (~6–8 weeks of age and a weight of about 20–26 g). All animals were housed 3–5 per cage and maintained on a 12-hour light/dark cycle, in a humidity- and temperature-controlled room with water and food available *ad libitum*. Littermates of the same sex were randomly assigned to experimental groups.

METHOD DETAILS

Homology Modeling

In all crystal structures of mouse GIRK2 (PDB: 3SYA (Whorton and MacKinnon, 2011), 3SYQ (Whorton and MacKinnon, 2011), 4KFM (Whorton and MacKinnon, 2013)) thus far, the N terminus of GIRK2 (residues 50–55), which forms a part of the alcohol-binding pocket in the cytoplasmic domain, is disordered. Therefore, we constructed a homology model of GIRK2 based on the crystal structure of the homotetrameric mouse Kir2.1 (sequence identity of the cytoplasmic domain: 61%; PDB: 2GIX (Pegan et al., 2006)), which has a structured N terminus and a bound alcohol, methyl-pentane-diol (MPD), in each interface between the subunits. As this construct had the transmembrane helices removed, the N-terminal region of subunit 1 (residues 41–64) was modeled to attach to the core of subunit 2 (residues 189–370). To correct this rearrangement for the subsequent homology modeling, the N-terminal region of the subunits in the template structure were reassigned to their corresponding subunits. Initially, 50 models of homodimeric GIRK2 cytoplasmic domain (residues 52–74, 205–376), in absence of MPD, were generated using MODELLER (Šali and Blundell, 1993) v9.18 with the default settings. One model of the GIRK2 pocket with the least steric clashes with the crystallographic pose of MPD in the known structure (i.e., 2GIX) was used for virtual screening. Subsequently, models of heterodimeric GIRK1 (residues 40–63, 194–365)/GIRK2 cytoplasmic domain (with two alternative arrangements: GIRK1/2 and GIRK2/1) were generated and used for identifying important sites for GiGA1 binding.

Virtual Screening

All docking calculations were performed with the Schrödinger suites (Schrödinger, 2017a, 2017b). The model of homodimeric GIRK2 cytoplasmic domain was prepared by Glide Grid with the following settings: (i) aromatic CH hydrogens and halogen atoms were treated as hydrogen-bond donor and acceptor, respectively; (ii) hydrophobic constraint to Leu257 side-chain was used; (iii) hydrogen-bond constraints to Lys52 amide NH and Pro256 carbonyl O were used; and (iv) van der Waals radius was softened (scaled to 0.8) for atoms with partial charge exceeding 0.25e. Docking calculations were performed with Glide (Schrödinger, 2017a) using the SP accuracy mode. The OPLS3 force field (Harder et al., 2016) was used to parameterize both the ligands and receptor.

We virtually screened two small molecule libraries: the “Fragment-Like Tranche” from ZINC15 (Sterling and Irwin, 2015) (~714,000 “clean, in-stock” compounds, downloaded in 2016), and a subset of a small-molecule library (56,834 molecules) provided by the National Center for Advancing Translational Sciences (NCATS). The molecules were prepared and tautomerized at pH 7.2 by LigPrep (Schrödinger, 2017b). The 1,000 top-scoring compounds from each virtual screen were subjected to visual inspection, to discard likely false positive predictions related to the limitation of the docking programs, such as docking poses with high internal energies or unbound polar groups, as well as molecules with strained conformations (Schlessinger et al., 2011). Nine compounds from the ZINC15 library were initially purchased and tested. Subsequently, 13 compounds from the NCATS library were synthesized and tested.

Molecular Dynamics Simulation

Induced-fit docking (IFD) (Schrödinger, 2017a) was used to predict the binding mode of GiGA1 and its analogs in the alcohol binding site of GIRK1/GIRK2. We used Gaussian accelerated molecular dynamics (GaMD) simulations to predict the structural and functional effect of mutations in GIRK1/GIRK2 and its binding to GiGA1. To enhance the sampling of protein dynamics, we used Gaussian accelerated Molecular Dynamics (GaMD) simulation method (Miao, Feher and McCammon, 2015), available in Amber 18 (Case et al., 2005), to examine the cytosolic domain of the GIRK1/GIRK2 heterotetramer models generated by MODELLER (Sali and Blundell, 1993) in the forms of wild-type, R43I and D346A single-mutations, and R43I/D346A double-mutation. FF14SB force field (Case et al., 2005) and TIP3P water model (Jorgensen et al., 1983) were used to parameterize the simulation system. Bond to hydrogen atom was restrained to enable 2-fs time interval (Ryckaert et al., 1977) and a 10-Å cutoff for PME (Darden et al., 1993) and non-bond interactions were used. Two independent trajectories of the protein system were conducted with minimization and equilibration for 30 ns before the 300 ns NVT production run with PMEMD.CUDA (Lee et al., 2018). Backbone dihedral angle data of trajectories was extracted using CPPTRAJ (Roe and Cheatham, 2013) and was plotted as Ramachandran plot with an in-house script (<https://github.com/schlessinger-lab/RAMAPlot>) to examine the distribution of secondary structure of a residue throughout the GaMD trajectories. An updated definition of amino acid secondary structures (Porter and Rose, 2011) is used to describe the distribution of backbone dihedral angles in an area between α R-helix and β sheet, the hydrogen-bonded inversed γ -turn centered at $\text{Phi}(\phi), \text{Psi}(\psi) = -85^\circ, 78^\circ: \text{NH}(i+1) \cdots \text{O}=\text{C}(i-1)$.

Molecular Biology and Cell Culture

cDNAs for rat GIRK1 (P63251), mouse GIRK2 (P48542), mouse GIRK3 (P48543), and rat GIRK4 (P48548) were used. Heteromeric channels were studied using either cDNAs for tandem dimers connected by a short linker (GIRK1_GIRK2c, GIRK1_GIRK3) or co-expression of individual subunits (GIRK1 + GIRK4, GIRK2c + GIRK3). All heterotetrameric channels in the results are referred to as GIRK1/GIRK2, GIRK1/GIRK3, and GIRK1/GIRK4. Mutations were introduced into GIRK2c and GIRK1/GIRK2c tandem cDNAs using site-directed mutagenesis (QuikChange II XL, Agilent Technology) and confirmed by DNA sequencing. Human Embryonic Kidney 293T (HEK293T) cells were cultured in Dulbecco's modified Eagle's medium (DMEM Sigma-Aldrich, St. Louis, MO, USA) supplemented with 10% (v/v) Fetal Bovine Serum (FBS), 100 U/ml penicillin, 100 $\mu\text{g}/\text{ml}$ streptomycin and 1X Glutamax (ThermoFisher) in a humidified 37°C incubator with 5% CO_2 . Cells were plated onto poly-D-lysine (100 $\mu\text{g}/\text{ml}$; SigmaAldrich) coated 12-mm glass coverslips in 24-well plates and transiently transfected with cDNA using Lipofectamine 2000 (ThermoFisher). HEK293T cells were transfected with GIRK channel cDNAs: GIRK2 (0.5 μg), GIRK1/GIRK2 dimer (0.5 μg), or a series of GIRK1/GIRK2 mutants (0.5 μg) and eYFP cDNA (0.02 μg ; to identify transfected cells). For testing G-protein-dependent effect, GABA_{B1b} (0.25 μg), GABA_{B2} (0.25 μg) and PTX S1 cDNA (0.25 μg) were also included.

HEK293T Electrophysiology

For HEK293T cell recordings, whole-cell patch-clamp recordings were made as described previously (Bodhinathan and Slesinger, 2013). Borosilicate glass electrodes (Warner Instruments) of 3-6 M Ω were filled with an intracellular solution containing 130 mM KCl, 20 mM NaCl, 5 mM EGTA, 5.46 mM MgCl₂, 2.56 mM K₂ATP, 0.3 mM Li₂GTP and 10 mM HEPES (pH 7.4, ~300 mOsm). The extracellular '20K' solution contained 20 mM KCl, 140 mM NaCl, 0.5 mM CaCl₂, 2 mM MgCl₂, and 10 mM HEPES (pH 7.4, ~318 mOsm) (Aryal et al., 2009). Currents were elicited at 0.5 Hz with a voltage step to -120 mV from a holding potential of -40 mV, followed by a ramp voltage protocol (-120 mV to +50 mV, E_K = -50 mV with 20 mM K_{out}). K⁺ currents were measured at -120 mV with either extracellular solution or drug solution. Drugs were diluted into extracellular solution with a final concentration of 100 μM Baclofen, 1-200 μM GiGA1, 100 mg 1-propranolol (PrOH), 10 μM ML297 or 1 mM BaCl₂. The percent activation was calculated by measuring the amplitude of the basal (I_{basal}) and drug-induced current (I_{drug}) using the equation $\% = (I_{\text{drug}} - I_{\text{basal}}) / I_{\text{basal}}$. I_{basal} was defined as the Ba²⁺-sensitive current. Dose-response curve was fit with the Hill equation, as described previously (Glaaser and Slesinger, 2017). In some plots, the GiGA1-dependent activation of mutants was calculated as the ratio of GiGA1 to ML297 [(GiGA1-induced)/(ML297-induced)], and then normalized as a percentage of the WT ratio (% Normalized GiGA1 activation). The voltage-dependent activation was measured in response to a voltage-step from -40 mV to -120 mV.

Ex Vivo Slice Electrophysiology

Mice were sacrificed with isoflurane euthanasia and perfused with ice-cold recovery artificial cerebrospinal fluid (aCSF) containing the following: NMDG 92 mM, KCl 2.5 mM, NaHCO₃ 30 mM, NaH₂PO₄ 1.25 mM, HEPES 20 mM, Glucose 25 mM, sodium ascorbate 5 mM, Thiourea 2 mM, sodium pyruvate 3 mM, CaCl₂ 0.5 mM (pH 7.3), and MgSO₄ 10 mM, bubbled with 95% O₂/5% CO₂ (Ting et al., 2018). All aspects of animal care and experimentation were approved by the Institutional Animal Care and Use Committee (IACUC) at the Icahn School of Medicine at Mount Sinai. Coronal slices containing hippocampus (300 μm) were prepared in recovery aCSF as well. Next, brain slices were equilibrated for 15 min at 33°C, and 1h at room temperature (RT, ~22°C) in recovery aCSF, and then transferred to a recording chamber equipped with constant perfusion of aCSF (2ml/min) contained the following: NaCl 119 mM, D-glucose 11 mM, NaHCO₃ 26.2 mM, KCl 2.5 mM, MgCl₂ 1.3 mM, NaH₂PO₄ 1 mM, CaCl₂ 2.5 mM (pH 7.3) (Cruz et al., 2004). We added 100 μM GiGA1, 300 μM Baclofen (Sigma-Aldrich), 5 μM CGP55845 (Sigma-Aldrich) or 30 μM SCH23390 (Sigma-Aldrich) directly to the aCSF (Kuzhikandathil and Oxford, 2002; Montalbano et al., 2015; Rifkin et al., 2018). Neurons were visualized by infrared illumination on an Olympus fluorescent scope (BX51WI) and whole-cell patch-clamp recordings were made from neurons

in the CA1 region of hippocampus. Pyramidal neurons were identified by morphology and location. For measuring drug-induced currents, whole-cell voltage-clamp recordings were used, and currents were measured at -40 mV. Whole-cell current-clamp recordings were used to measure the resting membrane potential and firing patterns, induced injecting current steps, in response to drug application.

In Vivo Seizure Model

Mice were pre-injected i.p. with either GiGA1 (20, 40, 60 mg/kg), Valproic acid (VPA; 200 mg/kg), or vehicle (10% DMSO, 40% PEG300, and 5% Solutol). After 15–30 min, 60 mg/kg PTZ was injected i.p. to induce acute seizure and mice behaviors were recorded for 30 min with a video camera. This dose induced generalized seizures but was sublethal (Itoh and Watanabe, 2009). Tonic-clonic seizures in PTZ-injected mice occurred within the first 10 min. Convulsions were classified and scored according to modified Racine score (Racine, 1972; Itoh et al., 2004; Shimada and Yamagata, 2018) as follows: 0, normal; 1, immobilization, sniffing; 2, head nodding, facial and forelimb clonus (short myoclonic jerk); 3, continuous myoclonic jerk, tail rigidity; 4, generalized limbic seizures with kangaroo posture or violent convulsion; 5, continuous generalized seizures (tonic or clonic-tonic convulsions); 6, death. The mean seizure score and percent of time in tonic seizure were compared between the VPA (+ control for anticonvulsant), GiGA1, and the vehicle group ($n = 8$ mice/group).

Locomotor Activity Analysis

The locomotion data was obtained for 15 min following i.p. injection of either vehicle or GiGA1 (20, 40, 60 mg/kg). In brief, same groups of mice from *in vivo* seizure study were placed in the center of an activity field arena (30 × 30 cm) equipped with a camera above for 5 min to habituate. The initial video was transformed in an images-sequence corresponding to a reduced frame rate (2 fps). The distance traveled 5 min after drug administration as analyzed using Spot tracker function from FIJI.

In vivo Pharmacokinetics

20 mg/kg of GiGA1 was administered intraperitoneally (i.p.) with a single dose (2 mg/mL) prepared in 10% DMSO, 40% PEG300, 5% solutol and 45% water on the day of dosing or directly before dosing. Each cohort had three mice, and plasma was collected at 5 min, 15 min, 30 min, 1 h, 2 h, 4 h, 8 h, 12 h, and 24h post-dose. Approximately 0.025 mL of blood was collected via the dorsal metatarsal vein at each time point. Blood samples were then transferred into plastic microcentrifuge tubes containing heparin–Na as an anti-coagulant. Samples were then centrifuged at 4000 g for 5 min at 4°C to obtain plasma. Plasma samples were then stored in polypropylene tubes, quickly frozen, and kept at -75°C until analyzed by LC/MS/MS. The mouse was fully exsanguinated before brain collection. The brains were collected at specific time points, quick-frozen in an ice box and kept at $-75 \pm 15^{\circ}\text{C}$. The tissue samples were weighed and homogenized with water by tissue weight (g) to water volume (mL) ratio 1:3 before analysis. The actual concentration is the detected value multiplied by the dilution factor. The following pharmacokinetic parameters were measured: $T_{1/2}$, C_{\max} , T_{\max} , AUC_{last} , and AUC_{inf} and calculated brain/plasma ratio. Animals were also monitored during the in-life phase by once-daily cage-side observations.

QUANTIFICATION AND STATISTICAL ANALYSIS

For single or multiple comparisons, statistical differences were assessed using Student's Paired t test, one-way analysis of variance (ANOVA) or Mixed-effects model (REML) followed by Bonferroni post hoc test, two-way repeated-measured ANOVA with Dunnett's or Tukey's post hoc tests. All values are reported as mean \pm SEM or S.D., as indicate in legend. Statistical tests and details along with sample size are described in the figure legends/figures. All statistics were performed using Prism 8 (GraphPad).

Cell Reports, Volume 31

Supplemental Information

Identification of a G-Protein-Independent

Activator of GIRK Channels

Yulin Zhao, Peter Man-Un Ung, Gergely Zahoránszky-Kóhalmi, Alexey V. Zakharov, Natalia J. Martinez, Anton Simeonov, Ian W. Glaaser, Ganesha Rai, Avner Schlessinger, Juan J. Marugan, and Paul A. Slesinger



Figure S1. Sequence alignment for the three major domains of the alcohol pocket in GIRK1/GIRK2 channels Related to Figures 3 and 5. Amino acid mutations indicated for GIRK1 (orange) and GIRK2 (blue). Boxed residues indicate alcohol-sensitive site identified previously (Aryal et al., 2009). Cartoon shows one view of the alcohol pocket in a GIRK1/GIRK2 heterotetrameric channel.

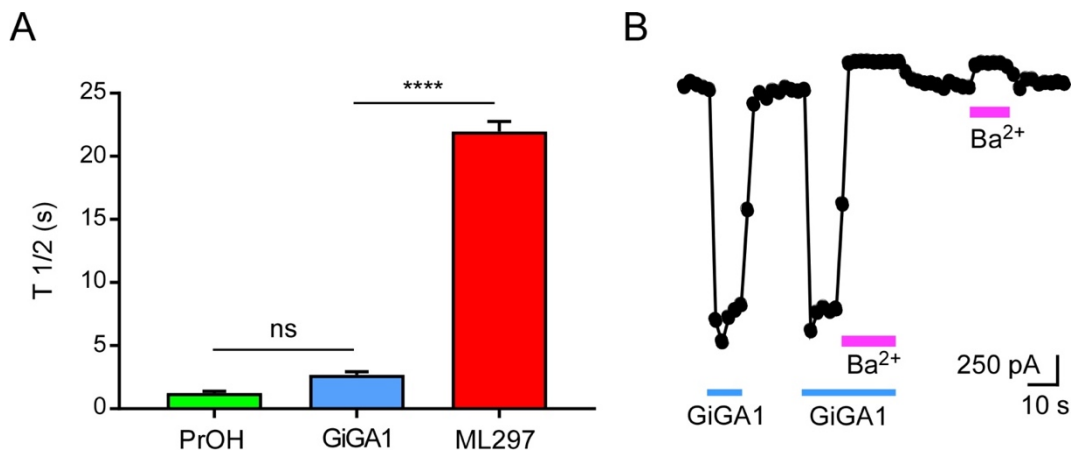


Figure S2. GiGA1 deactivation rates and inhibition by Ba²⁺. Related to Figure 2. (A) Bar graph shows mean deactivation rate (T_{1/2}) following ProOH (100 mM), GiGA1 (100 μM), and ML297 (10 μM)-induced activation of GIRK1/GIRK2 heterotetramers. **** P < 0.0001 for GiGA1 vs. ML297; One-way ANOVA: Bonferroni's Multiple Comparison post hoc test (F (2, 27) = 555.3; P < 0.0001) (n=10). ns: not significant. Error bars represent S.E.M.. (B) Trace show the current response to GiGA1 (100 μM), and/or Ba²⁺ (1 mM) for GIRK1/GIRK2 channels.

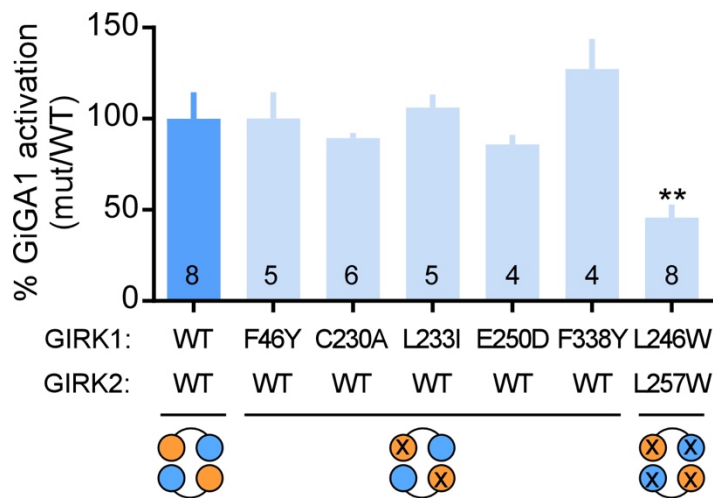


Figure S3. Percentage GiGA1 activation for mutants. Related to Figures 3 and 5. Bar graph shows the mean response of wild-type and mutant GIRK1/GIRK2 channels with GiGA1, normalized to the ML297-induced current. ** $P = 0.0017$ vs. GIRK1/GIRK2 WT; One-way ANOVA: Bonferroni's Multiple Comparison Test ($F(6, 28) = 8.477$; $P < 0.0001$). n indicated on graph. Error bars represent S.E.M..

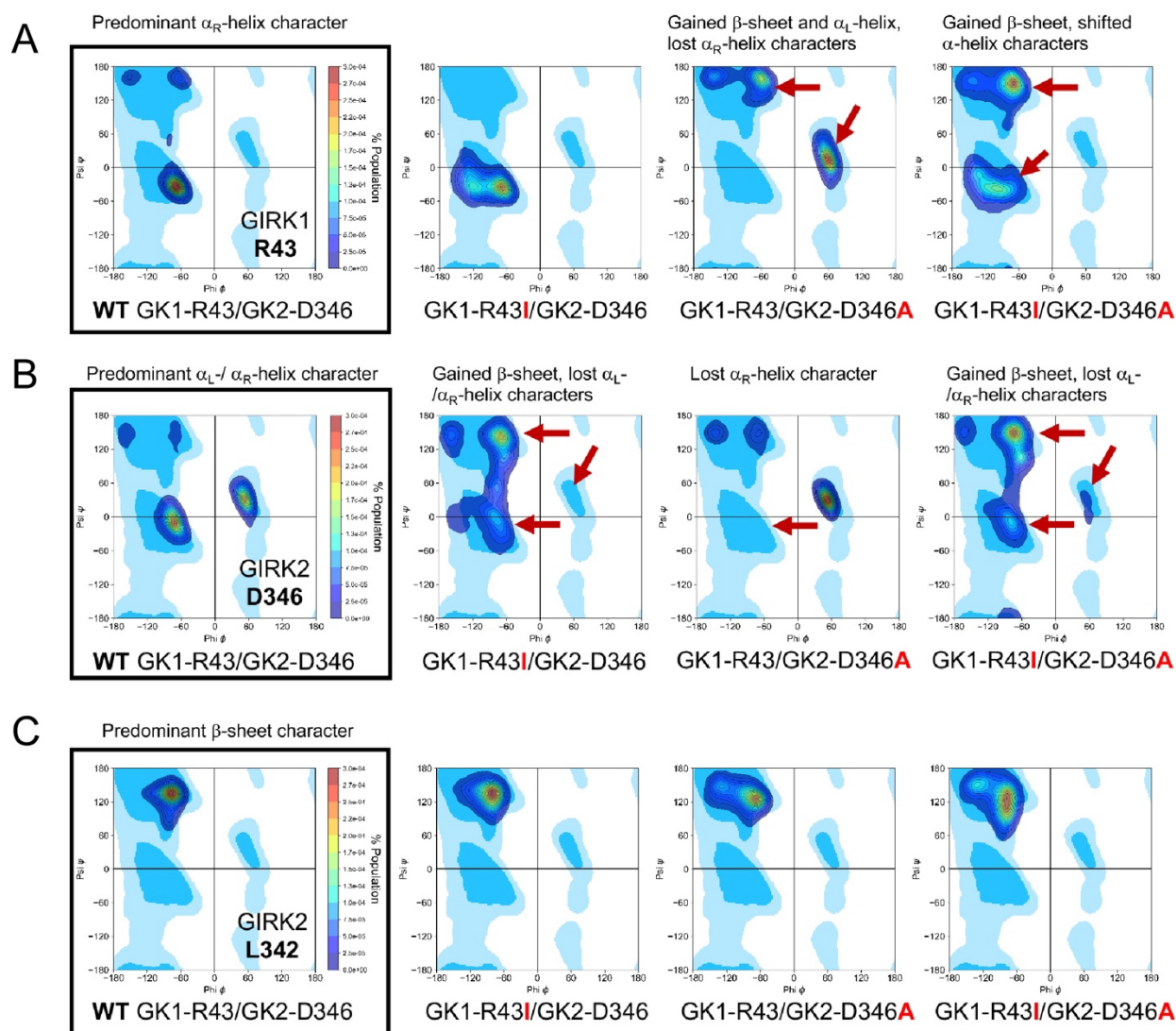


Figure S4. Molecular dynamics simulations of wild-type and mutant GIRK1/GIRK2 heterotetramer. Related to Figures 2, 3 and 5. Ramachandran plots of the mutated residues and a residue in the vicinity of mutations using Gaussian accelerated Molecular Dynamics (GaMD) simulations of GIRK1/GIRK2 heterotetramers. Distribution of the residue backbone dihedral angles is depicted as contoured density plot, in which the density is shown as a continuum of high to low in red to blue color, respectively. Known dihedral angle distribution of common amino acids is shown in the background as reference (light cyan and cyan area). **(A, B)** Single-mutation of GIRK1_{R43I} or GIRK2_{D346A} has slight effect on distribution of its own backbone dihedral angles (secondary structures). However, GIRK1_{R43I} single-mutation affects the distribution of secondary structures of GIRK2_{D346} and vice versa. Double-mutation has an additive effect on the backbone dihedral angles. **(C)** While GIRK2_{L342} is in the alcohol pocket and in the vicinity of the mutated residues, its secondary structure distribution in the simulation was unaffected by the mutations.

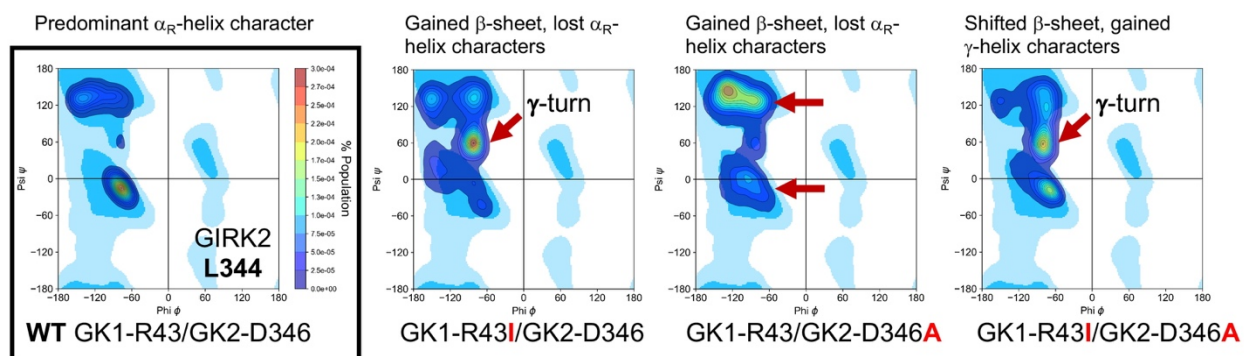


Figure S5. Molecular dynamics simulations of wild-type and mutant GIRK1/GIRK2 heterotetramers. Related to Figure 5. Ramachandran plots of GIRK2_{L344} in the presence of mutations in GaMD simulations of GIRK1/GIRK2 heterotetramers. Single- and double-mutations of GIRK1_{R43I} and GIRK2_{D346A} affect the distribution of GIRK2_{L344} secondary structures: GIRK2_{L344} lost the right-handed α_R -helix character while gaining β -sheet and inverted γ -turn characters.

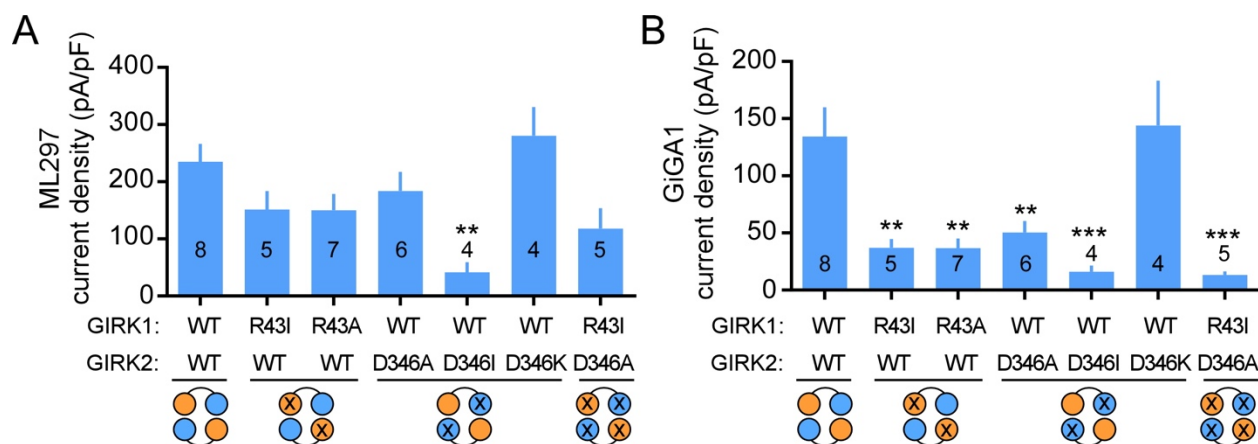


Figure S6. Current density for ML297- and GiGA1-activated currents. Related to Figure 5. Bar graphs show the mean current density for ML297 (A) and GiGA1 (B) induced responses for wild-type and mutant GIRK1/GIRK2 channels. (A) ** $P = 0.0025$ vs. GIRK1/GIRK2 WT; One-way ANOVA: Bonferroni's Multiple Comparison Test ($F(6, 32) = 4.354; P=0.0025$). (B) ** $P < 0.01$, *** $P < 0.001$ vs. GIRK1/GIRK2 WT; One-way ANOVA: Bonferroni's Multiple Comparison Test ($F(6, 32) = 8.244; P<0.0001$). n indicated on graph. Error bars represent S.E.M.

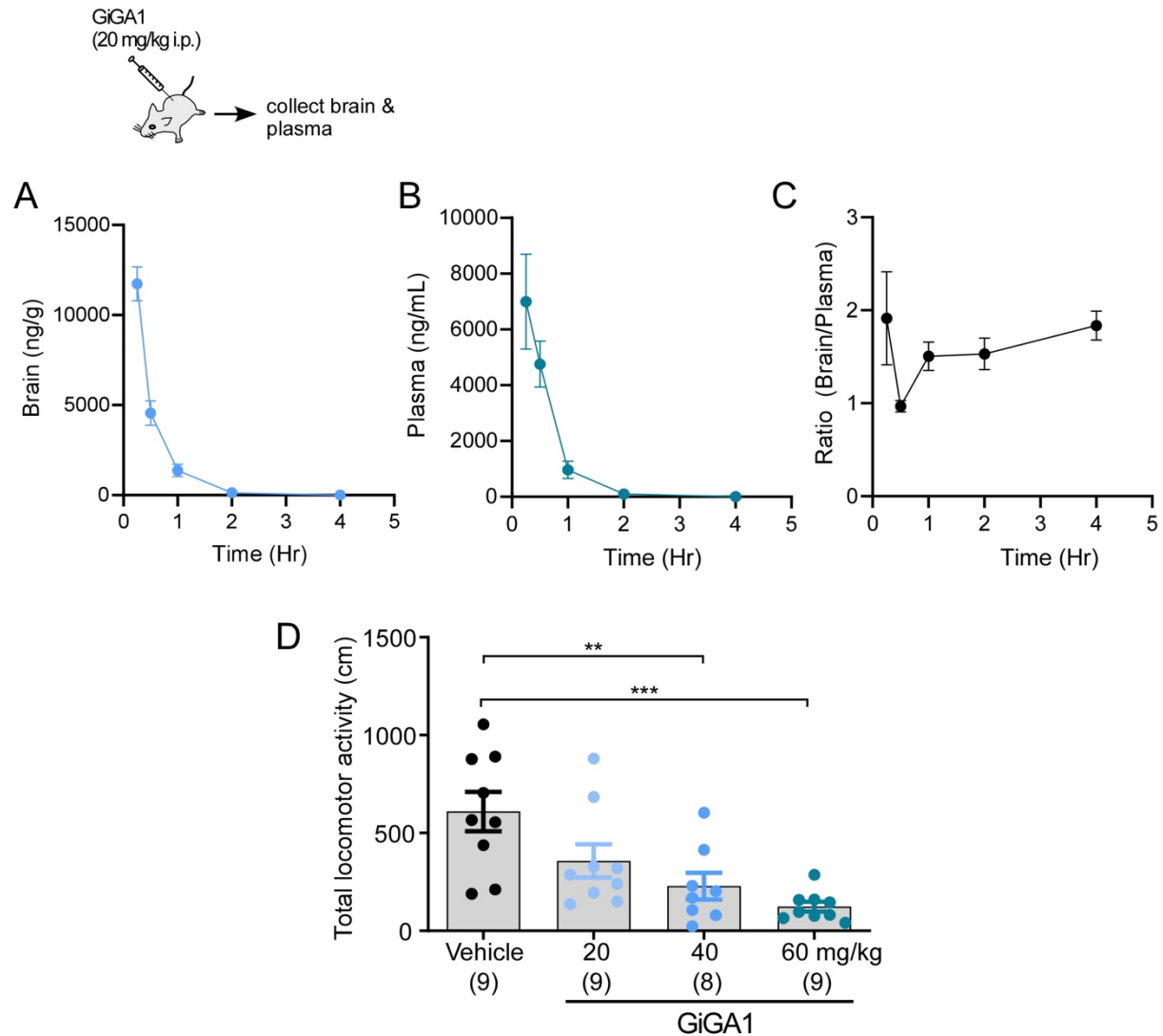


Figure S7. In vivo PK and effect on motor activity for GiGA1. Related to Figure 7 and STAR methods. (A-C) Pharmacokinetic (PK) profiles for GiGA1 *in vivo*. Levels of GiGA1 were measured in brain (A) and plasma (B) using LC/MS/MS, and are plotted against time after i.p. injection (n=3 mice per point). (C) Brain to plasma ratio is calculated over time. Note that GiGA1 has high brain permeability. (D) Bar graph shows total distance mice traveled 5 min after injection of vehicle or the indicated doses of GiGA1. ** $P = 0.0042$, *** $P = 0.0002$ vs. Vehicle; One-way ANOVA: Bonferroni's Multiple Comparison Test ($F(3, 31) = 7.856$; $P = 0.0005$). n indicated on graph. Error bars represent S.E.M..

Table S1: List of chemical compounds

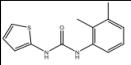
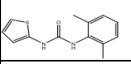
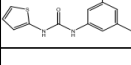
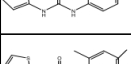
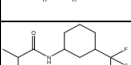
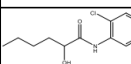
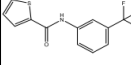
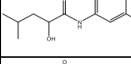
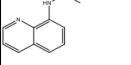
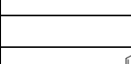
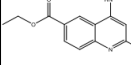
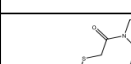
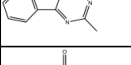
Name	NCATS ID	Chemical Name	
NCATS_1	proprietary		
NCATS_2	NCGC00113365-01		1-(2,3-dimethylphenyl)-3-(thiophen-2-yl)urea
NCATS_2.1	MLS000093627		1-(2,6-dimethylphenyl)-3-(thiophen-2-yl)urea
NCATS_2.2	NCGC00113368		1-(3,5-dimethylphenyl)-3-(thiophen-2-yl)urea
NCATS_2.3 / GIGA1	NCGC00092666		1-(2-methylphenyl)-3-(thiophen-2-yl)urea
NCATS_2.4	NCGC00113341		1-(2,4-dimethylphenyl)-3-(thiophen-2-yl)urea
NCATS_3	NCGC00262920-01		N-(3-(trifluoromethyl)cyclohexyl)isobutyramide
NCATS_4	NCGC00168723-01		N-(2-chloro-5-(trifluoromethyl)phenyl)-2-hydroxyhexanamide
NCATS_5	NCGC00229669-01		N-(3-(trifluoromethyl)phenyl)thiophene-2-carboxamide
NCATS_6	NCGC00168728-01		N-(2-chloro-5-(trifluoromethyl)phenyl)-2-hydroxy-4-methylpentanamide
NCATS_7	NCGC00161731-01		N-(quinolin-8-yl)acetamide
NCATS_8	proprietary		
NCATS_9	proprietary		
NCATS_10	NCGC00099858-01		3-((6-(ethoxycarbonyl)-2-methylquinolin-4-yl)amino)benzoic acid
NCATS_11	proprietary		
NCATS_12	MLS000041587-02		1-(3,4-dihydroquinolin-1(2H)-yl)-2-((2-methylbenzofuro[3,2-d]pyrimidin-4-yl)thio)ethan-1-one
NCATS_13	MLS001005104-02		2-((5-amino-1H-1,2,4-triazol-3-yl)thio)-N-(1,2,3,4-tetrahydronaphthalen-1-yl)acetamide

Table S1: List of chemical compounds and their structures screened in this study. Related to Figures 1E and 2A.